Logarithmic scaling of the collapse in the critical Keller–Segel equation

2013 Nonlinearity 26 3011

(http://iopscience.iop.org/0951-7715/26/11/3011)

IOP PUBLISHING NONLINEARITY

Nonlinearity **26** (2013) 3011–3041 doi:10.1088/0951-7715/26/11/3011

Logarithmic scaling of the collapse in the critical Keller–Segel equation

Sergey A Dyachenko, Pavel M Lushnikov and Natalia Vladimirova

Department of Mathematics and Statistics, University of New Mexico, Albuquerque, NM 87131, USA

Received 13 January 2013, in final form 28 July 2013
Published 18 October 2013
Online at stacks.iop.org/Non/26/3011

Recommended by L Ryzhik

Abstract

A reduced Keller–Segel equation (RKSE) is a parabolic–elliptic system of partial differential equations which describes bacterial aggregation and the collapse of a self-gravitating gas of Brownian particles. We consider RKSE in two dimensions, where solution has a critical collapse (blow-up) if the total number of bacteria exceeds a critical value. We study the self-similar solutions of RKSE near the blow-up point. Near the collapse time, $t = t_c$, the critical collapse is characterized by the $L \propto (t_c - t)^{1/2}$ scaling law with logarithmic modification, where L is the spatial width of the collapsing solution. We develop an asymptotic perturbation theory for these modifications and show that the resulting scaling agrees well with numerical simulations. The quantitative comparison of the theory and simulations requires several terms of the perturbation series to be taken into account.

Mathematics Subject Classification: 35A20, 35B40, 35B44

PACS numbers: 05.45.−a, 42.65.Jx, 87.18.Hf

(Some figures may appear in colour only in the online journal)

1. Introduction

In this paper we consider a reduced Keller–Segel equation (RKSE)

$$\begin{aligned} &\partial_t \rho = \Delta\rho - \nabla\cdot(\rho\nabla c),\\ &\Delta c = -\rho, \end{aligned} \tag{1}$$

which is the parabolic–elliptic system of partial differential equations (PDEs) for two scalar functions, $\rho = \rho(\boldsymbol{r}, t)$ and $c = c(\boldsymbol{r}, t)$. Here $\boldsymbol{r} \in \Omega \subseteq \mathbb{R}^D$ is the spatial coordinate in dimension D and t is the time. We assume that either $\Omega = \mathbb{R}^D$ or Ω is a bounded domain.

For $\Omega = \mathbb{R}^D$, we also assume that both ρ and c decay to zero as $|\boldsymbol{r}| \to \infty$. In the bounded domain case, we assume the zero flux condition for both ρ and c through the boundary $\partial\Omega$.

RKSE is the reduction of the well-known Keller–Segel model (also sometimes called Patlak–Keller–Segel model). See e.g. [1–17] and references therein. The Keller-Segel model was derived for the macroscopically averaged dynamics of bacteria and biological cells. Below we refer to bacteria and cell as synonyms. Bacteria often communicate through chemotaxis, when bacteria both secrete a substance called chemoattractant and move along the gradient of chemoattractant. The macroscopically averaged dynamics of bacteria is described by the bacterial density $\rho(\boldsymbol{r}, t)$ and the chemoattractant concentration $c(\boldsymbol{r}, t)$. Bacteria are self-propelled and, without the chemotactic clue, the center of mass of each bacteria typically experiences a random walk. The random walk is described by the first term (diffusion) on the right-hand side (rhs) of the first equation in (1). The diffusion of chemoattractant is described by the Laplacian term in the second equation. The term on the rhs of the second equation corresponds to the production rate of chemoattractant by the bacteria, which is proportional to the bacterial density. The second term on the rhs of the first equation characterizes the motion of bacteria towards large values of c. The motion of bacterial colonies is thus determined by competition between random-walk-based diffusion and chemotaxis-based attraction. For the convenience of the readers, we provide a more extensive description of the Keller–Segel model and the derivation of RKSE in appendix A.

Equation (1) also describes the dynamics of a gas of self-gravitating Brownian particles, which has applications in astrophysics including the problem of stellar collapse [11, 18–20]. In this case, the second equation in (1) is the Poisson equation for the gravitational potential, $-c$, while ρ is the gas density. (All units are dimensionless.) The first equation in (1) is a Smoluchowski equation for ρ. Below we refer to ρ and c as the density of bacteria and the concentration of chemoattractant, respectively, but all results below are equally true for the gravitational collapse of a gas of self-gravitating Brownian particles.

A solution of RKSE in dimension one ($D = 1$) is global (in time). For $D \geqslant 2$ (e.g. in dimensions two and three) a finite time singularity occurs [6] provided the initial condition is large enough. E.g. for dimension two ($D = 2$), a finite time singularity occurs for $N > 8\pi$, where $N = \int \rho \, \mathrm{d}\boldsymbol{r}$ is the total number of bacteria (in rescaled units) [14, 21]. Below we focus on unbounded domains $\Omega = \mathbb{R}^D$.

The formation of singularity in a finite time (blow-up) is a quite general phenomenon observed in many nonlinear systems including self-focusing in nonlinear optics, plasmas, hydrodynamics, and collapse of Bose–Einstein condensate [22]. Blow-up is often accompanied by a dramatic contraction of the spatial extent of solution, which is then called by collapse [22]. Collapse typically occurs when there are (i) self-attraction in nonlinear systems and, (ii) a conserved quantity, such as the spatial norm (e.g., L_2 or L_1 norm) of the solution. Such systems are often described by the nonlinear Schrödinger equation (NLSE) [23]:

$$\mathrm{i}\partial_t \psi + \nabla^2 \psi + |\psi|^2 \psi = 0 \tag{2}$$

for complex variable $\psi(\boldsymbol{r}, t)$. NLSE conserves the integral $P = \int |\psi|^2 \mathrm{d}\boldsymbol{r}$ and supports collapse for $D \geqslant 2$. Similarly, RKSE describes the attraction between brownian particles and conserves L_1 norm of ρ as well as RKSE admits collapse for $D \geqslant 2$.

A collapse in RKSE corresponds to the aggregation of bacterial colonies in biological applications and gravitational collapse for self-gravitating Brownian particles. Aggregation is a first step to a formation of multicellular organisms and quite important in biological applications [7]. E.g., the evolution of a low-density *Escherichia coli* bacteria colony in a petri dish is about one day [5]. However, if the bacterial density is locally high then bacteria aggregate on a timescale of several minutes [5]. Thus the aggregation has an explosive character

(see more details on that in appendix A). Near singularity the Keller–Segel model is not applicable when typical distance between bacteria is about or below the size of bacteria. In that regime a modification of the Keller–Segel model was derived from microscopic stochastic dynamics of bacteria [24–26]. That modified model prevents collapse due to excluded volume constraint (different bacteria cannot occupy the same volume). Here however the original RKSE without regularization is considered.

Collapses in NLSE and RKSE have much common, as detailed in reference [14]. E.g., the number of particles P in NLSE has a similar meaning to the number of bacteria N in RKSE. One can also recall that $|\psi|^2$ is the probability density in quantum mechanics. In two dimensions ($D = 2$), the critical number of particles, $P_c = 11.70\ldots$ (for NLSE), or the critical number of bacteria, $N_c = 8\pi$ (for RKSE), determine the boundary between collapsing and non-collapsing regimes in both systems [6, 27–32]. Collapse in the critical dimension $D = 2$ is strong for both RKSE and NLSE, which means that a finite number of bacteria (particles) is trapped within the collapsing spatial region. For the supercritical case ($D > 2$), collapse in both RKSE and NLSE is weak. Weak collapse implies that the collapse is so fast that particles (bacteria) cannot keep up with the collapse rate. Then a vanishing number of bacteria (particles) are trapped inside the collapsing region in the limit $t \to t_c$.

1.1. Summary of results

In this paper, we focus on the 2D self-similar solution of RKSE, equation (1). We assume that the spatial location of the collapse is $\boldsymbol{r} = 0$. Near t_c, in the neighborhood of the collapse, the solution of equation (1) has the following radially symmetric form:

$$\begin{aligned} &\rho = \frac{1}{L(t)^2}\frac{8}{(1+y^2)^2}, \\ &c = -2\ln(1+y^2), \\ &y = \frac{r}{L(t)}, \qquad r := \boldsymbol{r}, \\ &L(t) \to 0 \qquad \text{for} \quad t \to t_c, \end{aligned} \tag{3}$$

where ρ and c are defined above. Here, $L(t)$ is the time-dependent spatial width of solution. We also refer to $L(t)$ as the collapse width. (We sometimes omit the argument of L for brevity.) The self-similar form (3) is valid in the limit $t \to t_c$ in the small spatial neighborhood of the collapse point. This local applicability of the self-similar solution is typical for collapses in numerous nonlinear systems [22].

A number of different scalings for $L(t)$ have been proposed. First is the scaling,

$$L(t) = c_1\sqrt{t_c - t}\,\mathrm{e}^{-\sqrt{-\frac{\ln(t_c-t)}{2}}}[-\ln(t_c - t)]^{(1/4)(-\ln(t_c-t))^{-1/2}}, \tag{4}$$

where c_1 is the unknown constant. This scaling was derived in [4] using formal matched asymptotic expansion of RKSE near (3).

The second scaling,

$$L(t) = 2\mathrm{e}^{-\frac{2+\gamma}{2}}\sqrt{t_c - t}\,\mathrm{e}^{-\sqrt{-\frac{\ln(t_c-t)}{2}}}, \tag{5}$$

was derived in [9, 14]. Here $\gamma = 0.577216\ldots$ is the Euler constant. In [9], the formal matched asymptotic expansion of RKSE was used. The approach in reference [14] was based on the expansion of the perturbation around the collapsing solution (3) in terms of the eigenfunctions of the linearization operator. References [9, 14] give different estimates of errors. The rigorous stability analysis of the scaling (5) (with the prefactor $2\mathrm{e}^{-(2+\gamma)/2}$ replaced by the arbitrary constant) was performed in the recent reference [17].

The third scaling,

$$L(t) = c_2\sqrt{t_c - t}\,e^{-\frac{1}{2}\sqrt{-\frac{\ln(t_c-t)\ln[-\ln(t_c-t)]}{2}}}, \tag{6}$$

where c_2 is the unknown constant, was obtained in reference [11] by somewhat heuristic arguments. (Also see [33] for more discussion.)

The scaling laws (4)–(6) share two main features: (i) the leading-order square-root dependence, $L(t) \propto \sqrt{t_c - t}$, and (ii) the logarithmic-type modifications of $L(t)$. These modifications are necessary for the building the theory of the collapse in the critical dimension (2D). Both features are strikingly similar to the critical collapse in the 2D NLSE [27–29, 32, 34–40]. Earlier simulations [8, 11] show that corrections to the leading-order scaling $L(t) \propto \sqrt{t_c - t}$ are necessary, but fail to determine the form of the corrections.

In this paper we go much beyond the accuracy of scaling laws (4)–(6). We derive a new scaling law that agrees with the direct simulations of RKSE. There are three main results in this paper.

Our *first main result* is that $L(t)$ is determined by the solution of the following ordinary differential equation (ODE):

$$\begin{aligned}
&\frac{\partial_\tau a}{a^2} = -\frac{2}{\ln\frac{1}{a}} + \frac{M}{(\ln\frac{1}{a})^2} + \frac{b_0}{(\ln\frac{1}{a})^3} + O\left(\frac{1}{(\ln\frac{1}{a})^4}\right),\\
&M = -2 - 2\gamma + 2\ln 2,\\
&b_0 = \frac{\pi^2}{3} - 2\ln^2 2 + 4\ln 2 + \gamma(-4 - 2\gamma + 4\ln 2).
\end{aligned} \tag{7}$$

The adiabatically slow quantity

$$a = -L(t)\partial_t L(t), \tag{8}$$

evolves over a new time scale described by a new variable, τ, defined as

$$\tau = \int_0^t \frac{dt'}{L(t')^2}. \tag{9}$$

Here and below, the notation $f(x) = O(x)$ means that there exists a positive constant C such that $|f| \leqslant C|x|$ as $x \to 0$. It follows from (9) that $\tau \to \infty$ as $t \to t_c$, so that $\tau(t)$ maps the collapse time $t = t_c$ into $\tau = \infty$ in full analogy with the 'lens transform' of NLSE [38, 41, 42]. The decrease of $L \to 0$ as $t \to t_c$ implies that $a > 0$, and the logarithmic modification of $L(t) \propto \sqrt{t_c - t}$ scaling results in $a \to 0$ as $t \to t_c$. The logarithmic modification also makes a a slow function of $(t_c - t)^{1/2}$, compared with L. These scalings, as well as the definition of a, are in qualitative analogy with the scaling for NLSE collapse.

Our *second main result* is that the asymptotic solution of (7) in the limit $t \to t_c$, together with (8) and (9), is given by

$$\begin{aligned}
&L(t) = 2e^{-\frac{2+\gamma}{2}}\sqrt{t_c - t}\,\exp\left\{-\sqrt{-\frac{\ln\beta(t_c - t)}{2}} + \frac{-1 + b\ln x}{2x}\right.\\
&\qquad\left. + \frac{-1 + 2b + 2\tilde{M}(1 - b\ln x)}{4x^2} + O\left(\frac{1}{x^2}\right) + O\left(\frac{(\ln x)^2}{x^3}\right)\right\},\\
&x = \sqrt{-2\ln\beta(t_c - t)} - \tilde{M},\\
&\tilde{M} = -2 - \gamma + \ln 2,\\
&b = 1 + \frac{\pi^2}{6},
\end{aligned} \tag{10}$$

$$\beta = 2\exp\left\{2l^* - \frac{\tilde{M}^2}{2}\right\},$$

$$l^* = -\ln L_0 - \frac{1}{4}\ln^2 a_0 + \frac{\tilde{M}+1}{2}\ln a_0 - \frac{b}{2}\left(\ln\ln\frac{1}{a_0} + \frac{1}{\ln\frac{1}{a_0}}\right),$$

$$L_0 := L(t_0), \qquad a_0 := a(t_0) = -L(t_0)\partial_t L(t_0).$$

This scaling was presented without derivation in [43]. The time $t = t_0 < t_c$ is chosen arbitrarily, provided that at $t = t_0$, the solution is close to the self-similar form (3). (More details about choice of t_0 are given at the end of section 5 and in figure 1.) It is seen from (10) that $L(t)$ depends on the initial values $L(t_0)$ and $\partial_t L(t_0)$. The order of error terms in (10) are discussed below, after equation (92).

Our *third main result* is the comparison of (10) with direct numerical simulations of RKSE. Figure 1 shows excellent agreement between the theory and simulations. In the limit $t \to t_c$, the new scaling (10) asymptotically reduces to (5). We demonstrate, however, that while (5) is asymptotically correct, it is in quantitative agreement with both (10) and the direct RKSE simulations only for unrealistically small values of L. For example, the relative difference between (10) and (5) falls below 7% for the parameters of the simulation shown in figure 1 with $N/N_c = 1.0125$ provided $L \lesssim 10^{-116}$. It corresponds to

$$t_c - t \lesssim 10^{-218}. \tag{11}$$

That estimate is obtained by decreasing the numerical value of $t_c - t$ so that the relative difference between (10) and (5) falls below 7%. A stricter requirement on the relative error makes the estimate even more challenging. For example, 1% of the relative error is achieved for $N/N_c = 1.025$ provided $L \lesssim 10^{-5998}$ which corresponds to

$$t_c - t \lesssim 10^{-11893}. \tag{12}$$

In contrast, the scaling (10) is accurate starting from a moderate decrease of $L(t)$ from the initial value $L(0)$. Figure 2 shows the simulation with $N = 1.0125N_c$, where (10) is accurate (with the relative error $\lesssim$7%) for $L(t)/L(0) \lesssim 0.15$. In our simulations shown in figure 1, we typically reached values of $t_c - t$ down to 10^{-16} keeping high numerical precision. Sections 5 and 6 discuss these simulations and relative errors in more details.

1.2. Outline of the paper

The paper is organized as follows. In section 2 we consider general properties of collapses in RKSE and their analogies with the collapses in NLSE. In section 3 we study a collapsing self-similar solution of RKSE. We write the self-similar solution as a rescaled steady-state solution in new 'blow-up' variables. In these variables, the self-similar solution transforms into the approximate steady-state solution. The full collapsing solution evolves slowly about the steady-state solution, and depends on the small adiabatically slow parameter a defined in (8). We use a gauge transformation to a new dependent variable for perturbations about the self-similar solution. The gauge transformation brings the linearization operator about the self-similar solution to a self-adjoint form. In section 4 we discuss the spectrum and eigenfunctions of the linerization operator. In section 5 we expand the perturbations about the self-similar solution into eigenfunctions of the self-adjoint linearization operator, in order to derive a set of amplitude equations for the coefficients of the expansion. Compatibility conditions to ensure an adiabatic form of the expansion result in the ODE (7). In section 6, we solve equation (7) to derive the scaling (10). In section 7, we describe the simulation algorithm and the procedure for the extraction of the parameters of collapsing solutions from simulations. In section 8,

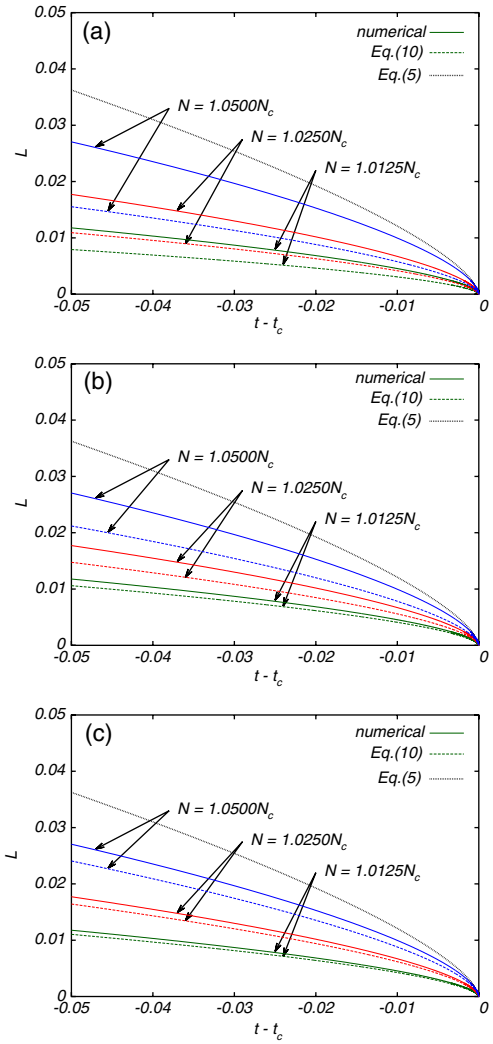

Figure 1. Dependence $L(t)$ obtained from the numerical simulations of RKSE (solid lines) is compared to the scaling (5) (dotted line) and to the scaling (10) (dashed lines). The lines of different colors correspond to different initial conditions (different values of N). Different panels show the different orders of the scaling in the exponent of the first equation of (10): (*a*) the terms up to $O(x^0)$ are taken into account; (*b*) the terms up to $O(x^{-1})$ are taken into account; (*c*) the terms up to $O(x^{-2})$, i.e. all terms except the error term $O(\ldots)$, are taken into account. Convergence of the analytical results to the numerical results with increase of the order in inverse power of x is clearly seen in (*a*)–(*c*). The relative difference between numerical and analytical results in (*c*) decreases with the decrease of $(N - N_c)/N_c > 0$ down to $\lesssim 6\%$ for the smallest shown value $N/N_c = 1.0125$. In simulations the initial conditions are chosen in the spatial Gaussian form as described in section 7.

the main results of the paper and future directions are discussed. In appendix A, we provide an extensive description of the Keller–Segel model and derive the RKSE. In appendix B, we provide the explicit expressions for the calculation of the scalar products from section 5; these expressions are obtained by using the asymptotic expansions of the Meijer G-function and the Γ-function.

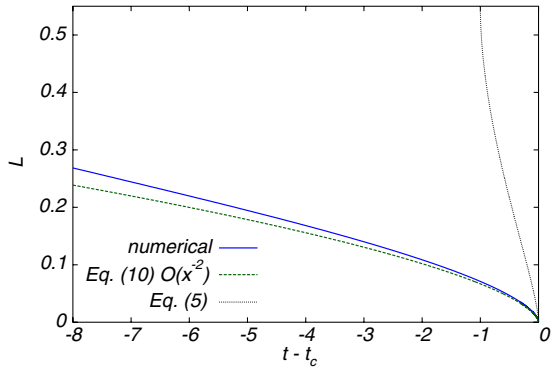

Figure 2. Dependence $L(t)$ during the time interval significantly exceeding the time interval of self-similar regime. The solid line shows the results of the numerical simulations for $N = 1.0125N_c$, the dotted line shows the scaling (5), while the dashed line shows the scaling (10). The six-fold decrease of L from the initial value $L(0) = 0.993\,339$ already gives a good agreement between numerical simulation and (10), with relative difference between them $\lesssim 7\%$ for $L < 0.15$. The scaling (5) agrees with simulation only in order of magnitude for $L \simeq 0.15$. Figure 1(*c*) shows the same curves for $N = 1.0125N_c$ zoomed-in to the origin.

2. Collapse of RKSE and NLSE

Equation (1) has a form of a conservation law

$$\partial_t \rho = -\nabla \cdot \Gamma, \tag{13}$$

where Γ is the flux of the bacterial density given by

$$\Gamma = -\rho \nabla \Big[\ln \rho - c \Big], \tag{14}$$

and $c(\boldsymbol{r})$ is determined by the fundamental solution $E(\boldsymbol{r}, \boldsymbol{r}')$ of the Poisson equation. The 2D case considered here implies that

$$c(\boldsymbol{r}) = -\int E(\boldsymbol{r}, \boldsymbol{r}')\rho(\boldsymbol{r}')\,\mathrm{d}\boldsymbol{r}', \qquad E(\boldsymbol{r}, \boldsymbol{r}') = \frac{1}{2\pi} \ln |\boldsymbol{r} - \boldsymbol{r}'|. \tag{15}$$

equation (15) allows to rewrite equation (1) as a closed integro-differential equation for ρ. The integral term in that equation originates from (15) and represents the non-locality of interaction due to diffusion of chemoattractant.

Assuming decaying boundary conditions at infinity, we obtain the conservation of the total number N of bacteria:

$$N = \int \rho(\boldsymbol{r})\mathrm{d}\boldsymbol{r} = \text{const}. \tag{16}$$

One can also define a Lyapunov functional

$$\mathcal{E} = \int \left[\rho(\boldsymbol{r}) \ln \rho(\boldsymbol{r}) - \rho(\boldsymbol{r}) - \frac{\rho(\boldsymbol{r})c(\boldsymbol{r})}{2} \right] \mathrm{d}\boldsymbol{r}, \tag{17}$$

and represent equation (1) in a gradient form

$$\partial_t \rho = \nabla \cdot \left(\rho \nabla \frac{\delta \mathcal{E}}{\delta \rho} \right), \qquad \frac{\delta \mathcal{E}}{\delta \rho} = \ln \rho - c, \tag{18}$$

where the Lyapunov functional $\mathcal{E}$ is a non-increasing function of time

$$\frac{\mathrm{d}\mathcal{E}}{\mathrm{d}t} = -\int \frac{\Gamma^2}{\rho}\,\mathrm{d}\boldsymbol{r}. \tag{19}$$

Functional $\mathcal{E}$ is conserved only for a steady-state solutions with zero flux $\Gamma = 0$.

Although equation (1) is a gradient non-Hamiltonian system (as follows from (18)), it has many striking similarities with NLSE (2) which can be written in a Hamiltonian form $\mathrm{i}\partial_t\psi = \delta H/\delta\psi^*$ with the Hamiltonian

$$H = \int \left[|\nabla\psi|^2 - \frac{|\psi|^4}{2}\right]\mathrm{d}\boldsymbol{r}. \tag{20}$$

To prove existence of collapse in RKSE one can use a positive-definite quantity $A = \int r^2\rho\,\mathrm{d}\boldsymbol{r}$, which determines the mean square width of bacterial density distribution [21, 44]. Vanishing of A guarantees the existence of collapse because of conservation of N. The proof of collapse existence for NLSE in $D = 2$ is based on a virial identity [28, 29]:

$$\partial_t^2 B = 8H. \tag{21}$$

Here $B := \int r^2|\psi|^2\mathrm{d}\boldsymbol{r}$ and H is defined in (20). If $H < 0$ then the positive-definite B turns negative in a finite time as follows from (21). It means that the negative value of the Hamiltonian is the sufficient condition for the collapse in NLSE. We also recall that in the quantum mechanical interpretation of NLSE, $|\psi|^2$ is the probability density of number of particles, i.e. the analogue of ρ in RKSE. Thus A from RKSE is the analogue of B in NLSE. However, RKSE is the non-Hamiltonian system and the direct analogy with a virial theorem for B does not work. Instead one can calculate a time derivative of A using equations (1) and (15), integration by parts, and vanishing boundary conditions at infinity. For $D = 2$, this procedure gives

$$\partial_t A = 4N - \frac{1}{2\pi}\int 2\boldsymbol{r}\cdot(\boldsymbol{r}-\boldsymbol{r}')\frac{\rho(\boldsymbol{r})\rho(\boldsymbol{r}')}{|\boldsymbol{r}-\boldsymbol{r}'|^2}\,\mathrm{d}\boldsymbol{r}\,\mathrm{d}\boldsymbol{r}' = 4N - \frac{N^2}{2\pi}. \tag{22}$$

Here we also used symmetrization over $\boldsymbol{r}$ and $\boldsymbol{r}'$. One concludes from (22) that $A_t < 0$ for $N > 8\pi$ and A turns negative in a finite time. That condition defines the critical number of bacteria

$$N_\mathrm{c} = 8\pi \tag{23}$$

because $A < 0$ proves the existence of collapse by contradiction (A is the positive-definite).

The existence of the critical number of bacteria (23) is another similarity with NLSE, where the critical number of particles $P_\mathrm{c} = \int|\psi|^2\mathrm{d}\boldsymbol{r} \simeq 11.70\ldots$ The difference between collapses in NLSE and RKSE is that according to (22) for RKSE, any initial condition with $N > N_\mathrm{c}$ develops into the collapsing solution in a finite time, while for NLSE, $P > P_\mathrm{c}$ is the necessary condition for collapse but not the sufficient condition. Another qualitative difference between RKSE and NLSE is that RKSE is the integro-differential equation while NLSE is a partial differential equation (PDE). However, it was shown in references [45, 46] that the generalized virial identity allows to prove the collapse existence in an integro-differential equation of NLSE-type with non-local nonlinearity. This type of nonlinearity describes, e.g., Bose–Einstein condensate with non-local dipole–dipole interaction. Collapse of such condensate was recently achieved in experiment [47].

Qualitative similarities between collapses in RKSE and in NLSE can be also understood if we recall that RKSE is the mean-field approximation for the dynamics of self-gravitating gas of brownian particles, while NLSE is the mean-field approximation for the quantum dynamics of atoms with Bose statistics and attraction at ultra-cold temperatures. Thus both RKSE and

NLSE approximate the dynamics of gas of particles with attraction. The principle difference is that the dynamics of brownian particles (RKSE) is diffusive (originates the overdamped motion with random force), while the dynamics of Bose atoms is the quantum analogue of Newtonian mechanics. In both cases collapse occurs if the number of particles is large enough to cause attraction overcoming either quantum pressure (NLSE) or diffusion (RKSE).

3. Self-similar collapsing solution of the 2D RKSE

2D RKSE (1) is invariant under the scaling transformations $\rho(\boldsymbol{r},t) \to \frac{1}{L^2}\rho(\frac{1}{L}\boldsymbol{r},\frac{1}{L^2}t)$, $c(\boldsymbol{r},t) \to c(\frac{1}{L}\boldsymbol{r},\frac{1}{L^2}t)$ for any $L(t) \equiv L = \text{const} > 0$. Similar property holds for NLSE. The 2D RKSE has a static, radially symmetric solution

$$\begin{aligned} \rho_0 &= \frac{8}{(1+r^2)^2}, \\ c_0 &= -2\ln(1+r^2), \end{aligned} \tag{24}$$

which corresponds to the critical number of bacteria, $N(\rho_0) = N_c = 8\pi$. This property is another striking similarity with the ground state soliton solution $\psi = R(r)\mathrm{e}^{\mathrm{i}t}$, $R(r) \geqslant 0$ of NLSE containing exactly the critical number of particles, $P_c = \int R^2\,\mathrm{d}\boldsymbol{r}$.

Assume that collapse is centered at $r = 0$. Then the solution of RKSE in the limit $t \to t_c$ approaches a radially symmetric, self-similar solution. The self-similar solution has the form of the rescaled stationary solution (24) with a time-dependent scale (the collapse width) $L(t)$:

$$\begin{aligned} \rho(r,t) &= \frac{1}{L(t)^2}\rho_0\left(\frac{r}{L(t)}\right), \\ c(r,t) &= c_0\left(\frac{r}{L(t)}\right). \end{aligned} \tag{25}$$

The scale $L(t)$ approaches zero for $t \to t_c$.

To describe the radially symmetric solution we introduce the new dependent variable m as follows,

$$m(r,t) = \frac{1}{2\pi}\int_{|r'|\leqslant r} \rho(\boldsymbol{r}',t)\,\mathrm{d}\boldsymbol{r}', \tag{26}$$

which allows us to rewrite RKSE as the closed equation for m [4]:

$$\partial_t m = r\partial_r r^{-1}\partial_r m + r^{-1}m\partial_r m. \tag{27}$$

Here, $m(r,t)$ has the meaning of the mass (the number of bacteria) inside the circle of radius r (up to a factor 2π). Boundary condition for m at $r \to \infty$ is simply related to the total number of bacteria: $m|_{r=\infty} = N/(2\pi)$. In contrast to RKSE, equation (27) is PDE for m. This simplification is possible only for radially symmetric solutions of RKSE.

In terms of m, the steady-state solution (24) of RKSE takes the following form:

$$m_0 = \frac{4r^2}{1+r^2}, \tag{28}$$

and the self-similar solution (25) becomes

$$\begin{aligned} m_{\text{selfsimilar}} &= \frac{4y^2}{1+y^2}, \\ y &= \frac{r}{L}. \end{aligned} \tag{29}$$

The boundary condition at infinity gives the critical number of bacteria, $2\pi m_{\text{selfsimilar}}\big|_{y\to\infty} \to 8\pi = \text{const}$, It also indicates that bacterial collapse is strong because the number of bacteria trapped within the collapse is nearly constant.

Assuming a power law dependence $L(t) \propto (t_0 - t)^{\beta}$ of the collapse width in the self-similar solution (29) one concludes that all terms in equation (27) are of the same order provided $\beta = 1/2$, which is similar to NLSE where also the collapsing width $\propto (t_0 - t)^{1/2}$. Like for NLSE, the self-similar solution (29) is not an exact solution of equation (27). To account for the difference, it is necessary to consider the logarithmic correction to $L(t) \sim (t_0 - t)^{1/2}$: $L = (t_0 - t)^{1/2} f(\ln(t_0 - t))$, where $f(\ln(t_0 - t))$ is a slow function compared with $(t_0 - t)^{1/2}$. This slow function comes from the nearly exact balance between linear and nonlinear terms of RKSE (between diffusion and attraction). The same slow function allows to introduce a small parameter a, defined in (8), which is a slow function of $(t_0 - t)^{1/2}$ compared with L. The balance between linear and nonlinear terms of RKSE improves with decrease of $a \to 0$.

Based on the analogy with the critical NLSE, we introduce in equation (27) the new independent 'blow-up' variables [16]:

$$\begin{aligned} y &= \frac{r}{L}, \\ \tau &= \int_0^t \frac{\mathrm{d}t'}{L(t')^2}. \end{aligned} \tag{30}$$

These new variables transform equation (27) into the equation for a new unknown function

$$\varphi(y, \tau) \equiv m(r, t) \tag{31}$$

into the following equation

$$\partial_\tau \varphi = y\partial_y(y^{-1}\partial_y\varphi) + y^{-1}\varphi\partial_y\varphi - ay\partial_y\varphi, \tag{32}$$

where a is given by (8). The advantage of working in blow-up variables is that the collapse occurs at $\tau = \infty$ instead of $t = t_c$, so that the collapse time t_c is eliminated from consideration. Also, the function φ has bounded derivatives.

Figures 3(a) and (b) show that as $t \to t_c$, the density $\rho(r)$ grows near $r = 0$ while the tail of $\rho(r)$ is practically frozen for $r \gtrsim 3$ (on a timescale of collapse). In contrast, the solution in the blow-up variables is steady at $y \lesssim 1$ and is well-approximated by (24) and (25), as shown in figures 3(c) and (d). It is also seen that the deviation of solution from (24) moves away from the origin $y = 0$ as $t \to t_c$.

Based on our assumption that a is a slow function, it is natural to look at the solutions of equation (32) in the adiabatic approximation where one can neglect τ-derivative in the left-hand side (lhs) of equation (32). Then, assuming that $|a| \ll 1$, one can expand the solution of (32) in powers of a starting from (29) for the power zero. Unfortunately, the term $-ay\partial_y\varphi$ grows with y and violates the expansion for large y. So, the adiabatic approximation can only work locally and is restricted to not very large y, a situation which is familiar from the analysis of collapse in NLSE. This however does not create a problem because the behaviour at large y does not affect the self-similar solution near zero.

It is convenient to present a general solution of equation (32) in the following form [16]:

$$\varphi(y, \tau) = \frac{4y^2}{1 + y^2} + \mathrm{e}^{\frac{a}{4}y^2}\frac{y^2}{y^2 + 1}v(y, \tau), \tag{33}$$

where $v(y, \tau)$ includes all corrections with respect to the self-similar solution (29). Here, the factor $\mathrm{e}^{\frac{a}{4}y^2}$ (which plays a role of a gauge transform) is inspired by a somewhat similar factor $\mathrm{e}^{-\mathrm{i}\frac{a}{4}y^2}$ in the self-similar solution of NLSE [32]. However, the absence of $-i$ in the exponent makes RKSE case quite distinct from NLSE case.

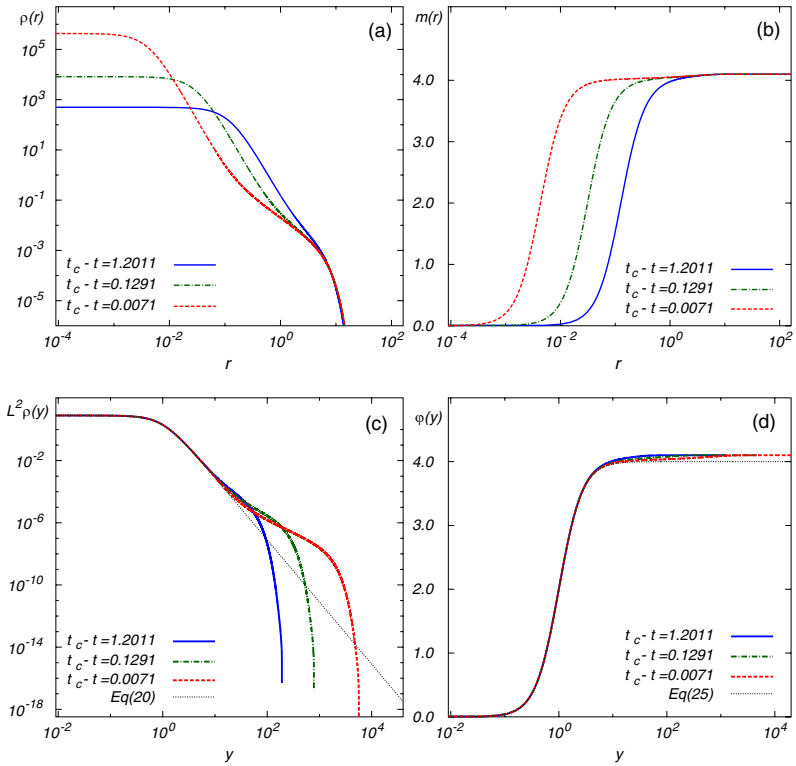

Figure 3. The spatial dependence of the density ρ (a), (c) and the mass m (b), (d) at different moments of time for the simulation with $N = 1.0250N_c$. In the top row (a), (b), the data are shown in simulation coordinates. In the bottom row (c), (d), rescaled density, $L^2\rho(y)$, and mass, $\varphi(y,\tau) \equiv m(r,t)$, are shown as functions of rescaled radius, $y = r/L$. In (a), notice the growth of $\rho(r)$ near the origin and a nearly steady tail. In (c), notice the convergence to the static solution (24), (25) in the growing neighborhood of $y = 0$. In loglog scale the deviation from that static solution has the form of a bump. The bump moves away from the origin as $t \to t_c$.

Substitution of (33) into (32) gives the following equation:

$$\partial_\tau v + \hat{\mathcal{L}}_a v = F. \tag{34}$$

Here

$$\hat{\mathcal{L}}_a = -\frac{1}{y^3}\partial_y y^3 \partial_y - \frac{8}{(1+y^2)^2} + \left[\frac{a^2}{4}y^2 - 2a + \frac{2a}{1+y^2}\right] \tag{35}$$

is the linear operator corresponding to the linearization of (32) with respect to (29). The right-hand side,

$$F = -\frac{\partial_\tau a}{4}y^2 v - \frac{8a}{y^2+1}e^{-ay^2/4} + \frac{ay^2v^2}{2(y^2+1)}e^{ay^2/4} + \frac{2v^2}{(y^2+1)^2}e^{ay^2/4} + \frac{yv\partial_y v}{y^2+1}e^{ay^2/4}, \tag{36}$$

is responsible for all other terms. These other terms include terms nonlinear in v, inhomogeneous terms, and linear terms. Generally, F cannot be zero because (29) is not an exact solution of (32) for non-zero a. Notice that up to now we have not made any approximations, so equations (33)–(36) are equivalent to equation (32).

The advantage of the definition (33) is that the operator $\hat{\mathcal{L}}_a = -\frac{1}{y^3}\partial_y y^3 \partial_y + V(y)$ has the form of the radially symmetric Schrödinger operator in spatial dimension four ($D = 4$) with

the potential

$$V(y) = -\frac{8}{(1+y^2)^2} + \left[\frac{a^2}{4}y^2 - 2a + \frac{2a}{1+y^2}\right]. \tag{37}$$

It means that $\hat{\mathcal{L}}_a$ is the self-adjoint operator with the scalar product

$$\langle \psi, \phi \rangle = \int_0^\infty \psi(y)\phi(y)\, y^3\, \mathrm{d}y. \tag{38}$$

The potential $V(y) \to \infty$ for $y \to \infty$, which ensures that $\hat{\mathcal{L}}_a$ has only discrete spectrum. This allows us to expand arbitrary v in a discrete set of eigenfunctions of $\hat{\mathcal{L}}_a$:

$$v = c_1\psi_1 + c_2\psi_2 + c_3\psi_3 + \cdots, \tag{39}$$

where $c_1(\tau),\ c_2(\tau),\ \ldots$ are $\tau-$dependent coefficients of the expansion (below we often omit argument τ for brevity), $\psi_j(y)$ are the eigenfunctions of $\hat{\mathcal{L}}_a$,

$$\hat{\mathcal{L}}_a\psi_j = \lambda_j\psi_j, \tag{40}$$

and λ_j are the respective eigenvalues. The eigenvalues are ordered starting from the lowest eigenvalue as $\lambda_1 < \lambda_2 < \cdots$. All eigenvalues are real and non-degenerate as discussed in the next section.

Note that the use of the scalar product (38) (which corresponds to the radially symmetric Schrödinger operator in $D = 4$) is simply an auxiliary mathematical trick, which is effective because the operator $\hat{\mathcal{L}}_a$ is self-adjoint with this scalar product. We remind that all solutions obtained below correspond to RKSE (1) with $D = 2$.

4. Spectrum of linearization operator

The eigenvalues (40) of the linearization operator $\hat{\mathcal{L}}_a$ are given by the following implicit expression:

$$\frac{\lambda + 2a}{2a}\left[\ln\frac{1}{a} - \Psi\left(-\frac{\lambda}{2a}\right) + K\right] = 1 + \mathrm{O}\left(a^{1/2}\ln\frac{1}{a}\right), \tag{41}$$

as it was proven in [15] using a rigorous version of the method of matched asymptotics. Here $K := \ln 2 - 1 - 2\gamma$, while Ψ is the digamma function, defined as $\Psi(s) = \frac{\mathrm{d}}{\mathrm{d}s}\ln\Gamma(s)$, where $\Gamma(s)$ is the gamma function.

Solving (41) for λ gives the spectrum of $\hat{\mathcal{L}}_a$, starting from the lowest eigenvalues, as follows

$$\begin{aligned}
\lambda_1 &= a\left(-2 + \frac{2}{\ln\frac{1}{a}} + 2(1+\gamma-\ln 2)\frac{1}{(\ln\frac{1}{a})^2} + \left[2(K+\gamma)^2 - \frac{\pi^2}{3}\right]\frac{1}{(\ln\frac{1}{a})^3}\right) + O\left(\frac{a}{(\ln\frac{1}{a})^4}\right),\\
\lambda_2 &= a\left(\frac{2}{\ln\frac{1}{a}} + 2(2+\gamma-\ln 2)\frac{1}{(\ln\frac{1}{a})^2} + \left[-4 + 2(K+\gamma)^2 - \frac{\pi^2}{3}\right]\frac{1}{(\ln\frac{1}{a})^3}\right) + O\left(\frac{a}{(\ln\frac{1}{a})^4}\right),\\
\lambda_3 &= a\left(2 + \frac{2}{\ln\frac{1}{a}} + (5+2\gamma-2\ln 2)\frac{1}{(\ln\frac{1}{a})^2}\right.\\
&\quad\left. + \left[2(1-3K-3\gamma) + 2(K+\gamma)^2 - \frac{\pi^2}{3}\right]\frac{1}{(\ln\frac{1}{a})^3}\right) + O\left(\frac{a}{(\ln\frac{1}{a})^4}\right),\\
&\ldots
\end{aligned} \tag{42}$$

Eigenfunctions ψ_j can be also approximated from the method of matched asymptotics.

In section 5 we need to calculate multiple integrals which involve ψ_j. For this purpose, it is more convenient to use the variational approximation for eigenfunctions obtained in [14]:

$$\begin{aligned}
\tilde{\psi}_1 &= \frac{8}{1+y^2}\mathrm{e}^{-ay^2/4},\\
\tilde{\psi}_2 &= \frac{8}{1+y^2}\left(1+\frac{ay^2}{2}-\frac{ay^2}{2}\ln(1+y^2)\right)\mathrm{e}^{-ay^2/4},\\
\tilde{\psi}_3 &= \frac{8}{1+y^2}\left(1+ay^2\left[-\frac{\pi^2\ln\frac{1}{a}}{\pi^2-12}+\frac{-12+\pi^2(2+\gamma-\ln 2)}{\pi^2-12}\right]\right.\\
&\quad \left.+ay^2\ln(1+y^2)\frac{12}{\pi^2-12}+\frac{a^2y^4}{4}\left[\ln\frac{1}{a}-3-\gamma+\ln 2-\frac{24}{\pi^2-12}\right]\right)\mathrm{e}^{-ay^2/4},
\end{aligned} \tag{43}$$

where $\tilde{\psi}_j$ means the variational approximation to ψ_j, $j=1,2,\ldots$. We estimate the accuracy of the variational approximation by calculating the variational approximation for the three lowest eigenvalues λ_1, λ_2, and λ_3 as $\lambda_j = \langle\tilde{\psi}_j, \hat{\mathcal{L}}_a\tilde{\psi}_j\rangle/\langle\tilde{\psi}_j,\tilde{\psi}_j\rangle$, $j=1,2,3$. These scalar products involve the calculation of integrals of the type described in appendix B. Expansion of the resulting expressions for integrals λ_1, λ_2, and λ_3 in inverse powers of $\ln\frac{1}{a}$ agrees with exact results (42) up to order $O(\frac{1}{(\ln\frac{1}{a})^2})$ for λ_1, λ_2 and up to order $O(\frac{1}{\ln\frac{1}{a}})$ for λ_3. This is the best result we are able to achieve with the variational approximation. This accuracy will be however sufficient to obtain (7).

5. Amplitude equations

Similar to (39), we expand v from (34) in a set of approximate variational eigenfunctions $\tilde{\psi}_j$, $j=1,2,\ldots$ as follows:

$$v=\sum_{j=1}^{\infty}c_j\tilde{\psi}_j, \tag{44}$$

where $c_j(\tau)$ are the coefficients of the expansion. In this section we derive a set of amplitude equations for $c_1(\tau)$, $c_2(\tau),\ldots$ from (44) which provide a solution of equation (34). We solve the amplitude equations exploiting the fact that, at the leading order in a, the solution of (32) is given by (29). (We used that fact in the definition of (33)). We expand all expressions below in integer powers of the small parameters a and $\frac{1}{\ln\frac{1}{a}}$, keeping the lowest non-trivial order of a and several orders of $\frac{1}{\ln\frac{1}{a}}$.

We assume the approximate orthogonality of the variational functions,

$$\langle\tilde{\psi}_i,\tilde{\psi}_j\rangle = O(a)\|\tilde{\psi}_i\|\|\tilde{\psi}_j\| \qquad \text{for} \quad i\neq j, \tag{45}$$

where $\|\tilde{\psi}_i\| := \langle\tilde{\psi}_i,\tilde{\psi}_i\rangle^{1/2}$, $i=1,2,\ldots$. Then, the scalar multiplication of (34) onto $\tilde{\psi}_j$ (with the scalar product (38)) results in

$$\begin{aligned}
&\langle\tilde{\psi}_j,\partial_\tau v\rangle+\langle\tilde{\psi}_j,\hat{\mathcal{L}}_a v\rangle-\langle\tilde{\psi}_j,F(v)\rangle\\
&\qquad=\|\tilde{\psi}_i\|^2\partial_\tau c_j+\sum_{i=1}^{\infty}c_i\langle\tilde{\psi}_j,\partial_\tau\tilde{\psi}_i\rangle+\sum_{i=1}^{\infty}c_i\langle\tilde{\psi}_j,\hat{\mathcal{L}}_a\tilde{\psi}_i\rangle-\langle\tilde{\psi}_j,F(v)\rangle=0.
\end{aligned} \tag{46}$$

Here, we neglect corrections from non-exact orthogonality (45) because, as we show later, these corrections are of the next order in a when compared with other terms in (46). In this section, all calculations of scalar products for (46) are based on integrals defined in appendix B for the

variational functions (43). For instance, the direct calculation for the variational functions (43) gives the following expressions:

$$\begin{aligned}
\|\tilde{\psi}_1\|^2 &= -32\ln a + 32(-1-\gamma+\ln 2) + O\left(a\ln a\right),\\
\|\tilde{\psi}_2\|^2 &= 32(\ln a)^2 + 32(1+2\gamma-2\ln 2)\ln a,\\
&\quad +\frac{16}{3}\left[\pi^2 + 6(\ln 2-1)\ln 2 + 6\gamma(\gamma+1-2\ln 2)\right] + O\left(a\ln a\right),\\
\|\tilde{\psi}_3\|^2 &= 64(\ln a)^2 + \frac{32\left(-108-48\gamma+13\pi^2+4\gamma\pi^2+48\ln 2-4\pi^2\ln 2\right)}{\left(-12+\pi^2\right)}\ln a\\
&\quad +\frac{1}{\left(-12+\pi^2\right)^2}32\Big[2\gamma^2\left(-12+\pi^2\right)^2 + \pi^4[23+\ln 2(-13+2\ln 2)])\\
&\quad -24\pi^2[13+\ln 2(-11+2\ln 2)] + 144(-1+\ln 2)(-7+2\ln 2)\\
&\quad -\gamma\left(-12+\pi^2\right)[108-48\ln 2+\pi^2(-13+4\ln 2)]\Big] + O\left(a(\ln a)^2\right).
\end{aligned} \tag{47}$$

We assume (based, e.g., on numerical simulations in [6, 8] and following reference [14]) that a is the adiabatically slow function of τ: $\partial_\tau a \ll a^2$. As mentioned above, we expand all quantities in the small parameters a and $\frac{1}{\ln\frac{1}{a}}$ (it is also seen in appendix B that all integrals involved in (46) expand into these parameters) keeping only a leading order in a and many enough terms in powers of $\frac{1}{\ln\frac{1}{a}}$. Then the adiabatic assumption $\partial_\tau a \ll a^2$ requires $\partial_\tau a = a^2 O(\frac{1}{\ln\frac{1}{a}})$. We introduce a normalized function $\tilde{a}_\tau := \frac{\partial_\tau a}{a^2}\frac{1}{\ln\frac{1}{a}} = O(1) + O(a)$. This allows to write $\partial_\tau a$ as an expansion in inverse powers of $\ln\frac{1}{a}$ only:

$$\partial_\tau a = a^2\,\frac{1}{\ln\frac{1}{a}}\,\tilde{a}_\tau, \qquad \tilde{a}_\tau = \tilde{a}_\tau^{(0)} + \tilde{a}_\tau^{(1)}\frac{1}{\ln\frac{1}{a}} + \tilde{a}_\tau^{(2)}\frac{1}{\left(\ln\frac{1}{a}\right)^2} + O\left(\frac{1}{(\ln\frac{1}{a})^3}\right), \tag{48}$$

where the coefficients $\tilde{a}_\tau^{(0)}$, $\tilde{a}_\tau^{(1)}$ and $\tilde{a}_\tau^{(2)}$ are $O(1)$ and do not depend on τ in the adiabatic approximation. Note that the subscript τ in these coefficients is *not* a partial derivative but rather indication that these are the expansion coefficients for $\tilde{a}_\tau$.

Assume that the expansion coefficients $c_1,\ c_2,\ c_3, \ldots$ in (44) are initially $O(1)$. A series expansion of equations (46) over small a, using equation (48) and dividing each jth equation by $\|\tilde{\psi}_j\|^2$, together with (47), result at the leading order in the following expressions

$$\begin{aligned}
&\partial_\tau c_1 + a - 2ac_1 + O\left(\frac{a}{\ln\frac{1}{a}}\right) = 0,\\
&\partial_\tau c_2 + O\left(\frac{a}{\ln\frac{1}{a}}\right) = 0,\\
&\partial_\tau c_3 + 2ac_3 + O\left(\frac{a}{\ln\frac{1}{a}}\right) = 0,\\
&\partial_\tau c_4 + 4ac_4 + O\left(\frac{a}{\ln\frac{1}{a}}\right) = 0.\\
&\ldots
\end{aligned} \tag{49}$$

Here, the terms $2a(j-2)c_j$, $j = 1, 2, 3$ originate from eigenvalues for $\tilde{\psi}_j$ (see equation (42)), while the term a in the first equation comes from the scalar product of $\tilde{\psi}_1$ with the second term in the right-hand side of (36). Also the contribution from $\partial_\tau\psi_j = (\partial_\tau a)\partial_a\psi_j$, $j = 1, 2, \ldots$ is included into $O(\ldots)$ term. It follows from equations (49) that the coefficient c_3 initially

decays exponentially (because $a > 0$) until it reaches the adiabatic, quasi-steady state with $c_3 = O(\frac{1}{\ln \frac{1}{a}})$. Our conjecture is that the other coefficients, $c_4, c_5, \ldots$, also decay exponentially (they correspond to the larger values λ_j, so that they are assumed to decay as $c_j \propto \exp[-2a(j-2)\tau]$, according to the linear terms in (34)). The lack of explicit expressions for $\tilde{\psi}_j$, $j \geqslant 4$ does not allow us to prove this statement. We conclude that, after an initial transient, the coefficients $c_3, c_4, \ldots$ reach the adiabatic state with their values

$$c_3, c_4, \ldots = O\left(\frac{1}{\ln \frac{1}{a}}\right). \tag{50}$$

Below we assume this adiabatic state.

In the first equation of (49) we assume that

$$c_1 = \frac{1}{2} + O\left(\frac{1}{\ln \frac{1}{a}}\right) \tag{51}$$

to avoid exponential growth of c_1 in τ. (Such artificial exponential growth would result in error in estimating t_c.)

We have now a freedom in selecting c_2, and we choose it so that $v \to 0$ for any y as $a \to 0$. According to (43), $\tilde{\psi}_1(y)|_{y=0} = \tilde{\psi}_2(y)|_{y=0} = 8$ so we set

$$c_2 = -\frac{1}{2} + O\left(\frac{1}{\ln \frac{1}{a}}\right). \tag{52}$$

In this case, $c_1\tilde{\psi}_1 + c_2\tilde{\psi}_2 = O(a)$ for $y = O(1)$, i.e. v in (33) vanishes with $a \to 0$, as we expect from the self-similar solution (29).

Equations (50), (51) and (52) justify the adiabatic approximation, which means that the coefficients $c_1, c_2, c_3, c_4, \ldots$ depend on τ only through a, and one can expand them in series of inverse powers of $\ln \frac{1}{a}$:

$$\begin{aligned}
c_1 &= \frac{1}{2} + \sum_{k=1}^{\infty} d_1^{(k)} \frac{1}{(\ln \frac{1}{a})^k} + O(a), \\
c_2 &= -\frac{1}{2} + \sum_{k=1}^{\infty} d_2^{(k)} \frac{1}{(\ln \frac{1}{a})^k} + O(a), \\
c_3 &= \sum_{k=1}^{\infty} d_3^{(k)} \frac{1}{(\ln \frac{1}{a})^k} + O(a), \\
&\ldots
\end{aligned} \tag{53}$$

where the expansion coefficients $d_i^{(j)} = O(1)$ for any i, j; the coefficients do not explicitly depend on τ in the adiabatic approximation.

It follows from (53) and (48) that

$$\partial_\tau c_j = O\left(\partial_\tau \frac{1}{\ln \frac{1}{a}}\right) = O\left(\frac{a}{(\ln \frac{1}{a})^3}\right), \qquad j = 1, 2, 3, \ldots. \tag{54}$$

Similar to derivation of equations (49), we now perform a series expansion of equations (46) into small a (but in contrast to the derivation of equations (49) we proceed to the higher

orders of expansion) using equations (47), (48), (53) to obtain following equations:

$$\partial_\tau c_1 + \frac{a}{\ln\frac{1}{a}}\left[\frac{\tilde{a}_\tau^{(0)}}{2} - 2d_1^{(1)}\right] + \frac{a}{(\ln\frac{1}{a})^2}\left[\frac{\tilde{a}_\tau^{(1)}}{2} + 2d_1^{(1)} - 2d_1^{(2)} + 2d_2^{(1)} - \tilde{a}_\tau^{(0)}d_2^{(1)} + 2d_3^{(1)}\right] + O\left(\frac{a}{(\ln\frac{1}{a})^3}\right) = 0, \tag{55}$$

$$\partial_\tau c_2 + \frac{a}{\ln\frac{1}{a}}\left[-1 - \frac{\tilde{a}_\tau^{(0)}}{2}\right] + \frac{a}{(\ln\frac{1}{a})^2}\left[-1 - \frac{\tilde{a}_\tau^{(1)}}{2} + 2d_2^{(1)} + \tilde{a}_\tau^{(0)}(d_2^{(1)} - 2d_3^{(1)}) - \gamma + \ln 2)\right] + \frac{a}{(\ln\frac{1}{a})^3}\Big[-1 - \frac{\tilde{a}_\tau^{(2)}}{2} + 2d_1^{(1)} + (2 + \tilde{a}_\tau^{(0)})d_2^{(2)} + 6d_3^{(1)} + 4\tilde{a}_\tau^{(0)}d_3^{(1)} - 2\tilde{a}_\tau^{(1)}d_3^{(1)} - 2\tilde{a}_\tau^{(0)}d_3^{(2)} + \frac{\pi^2}{6} + \frac{24\tilde{a}_\tau^{(0)}d_3^{(1)}}{-12+\pi^2} - (\ln 2)^2 + d_2^{(1)}(4 + \tilde{a}_\tau^{(1)} + 2\gamma - 2\ln 2) + 2\ln 2 + \gamma(-2 - \gamma + 2\ln 2)\Big] + O\left(\frac{a}{(\ln\frac{1}{a})^4}\right) = 0, \tag{56}$$

$$\partial_\tau c_3 + \frac{a}{\ln\frac{1}{a}}\left[2d_3^{(1)}\right] + \frac{a}{(\ln\frac{1}{a})^2}\left[-1 + 2(1 + \tilde{a}_\tau^{(0)})d_3^{(1)} + 2d_3^{(2)}\right] + O\left(\frac{a}{(\ln\frac{1}{a})^3}\right) = 0. \tag{57}$$

Here we have neglected the expansion coefficients c_j for $j > 3$ by setting $c_4 = c_5 = c_6 = \cdots = 0$. In equations (55)–(57) we keep the necessary number of orders in $\frac{1}{\ln\frac{1}{a}}$ to obtain the closed expressions for the expansion terms in (48). Equations (55)–(57) can be viewed as the compatibility conditions which ensure that expansions (53) and (48) are correct, so that a is indeed the adiabatically slow variable.

It follows immediately from equation (57) in the order $\frac{a}{\ln\frac{1}{a}}$ that

$$d_3^{(1)} = 0, \tag{58}$$

and from equation (56) in the order $\frac{a}{\ln\frac{1}{a}}$ that

$$\tilde{a}_\tau^{(0)} = -2. \tag{59}$$

Then, from equation (55) in the order $\frac{a}{\ln\frac{1}{a}}$ we obtain

$$d_1^{(1)} = -\tfrac{1}{2}. \tag{60}$$

Using equations (56) and (58)–(60) we obtain in the order $\frac{a}{(\ln\frac{1}{a})^2}$ that

$$\tilde{a}_\tau^{(1)} = -2 - 2\gamma + 2\ln 2. \tag{61}$$

Using equations (55) and (58)–(61) we obtain in the order $\frac{a}{(\ln\frac{1}{a})^2}$ that

$$d_1^{(2)} = \tfrac{1}{2}(-2 + 4d_2^{(1)} - \gamma + \ln 2). \tag{62}$$

Similar, using equations (57) and (58)–(61) we obtain in the order $\frac{a}{(\ln\frac{1}{a})^2}$ that

$$d_3^{(2)} = \tfrac{1}{2}. \tag{63}$$

Equation (56) in order $\frac{a}{(\ln\frac{1}{a})^3}$ requires also to take into account $\partial_\tau c_2$ which is given by

$$\partial_\tau c_2 = -\frac{1}{2}\frac{a}{(\ln\frac{1}{a})^3} + O\left(\frac{a}{(\ln\frac{1}{a})^4}\right), \tag{64}$$

Table 1. Parameters of collapses at the time $t = t_0$ extracted from RKSE simulations (the same simulations are shown by solid lines in figure 1). For each simulation, the time t_0 is found by the criterion that the relative difference between numerical and analytical curves of figure 4 reduces down to 20% (see text for more details). These parameters are used together with the equation (10) to plot the dashed lines in figure 1.

N/N_c	$\tau(t_0)$	t_0	t_c	L_0	a_0	$\partial_\tau a(t_0)$
1.0125	117.557	11.5928	16.6541	0.19612	4.4824×10^{-3}	-1.1448×10^{-5}
1.025	120.310	7.2118	8.12305	0.10645	7.9058×10^{-3}	-3.4246×10^{-5}
1.05	41.728	3.3295	3.94247	0.13478	1.9794×10^{-2}	-2.6254×10^{-4}

according to (54) and (53).

Using equation (56) in order $\frac{a}{(\ln\frac{1}{a})^3}$ and (58)–(61), (63), (64) we obtain the closed expression

$$\tilde{a}_\tau^{(2)} = \frac{\pi^2}{3} - 2(\ln 2)^2 + 4\ln 2 + \gamma(-4 - 2\gamma + 4\ln 2). \tag{65}$$

Here, the unknown coefficient $d_2^{(1)}$ has been cancelled out identically.

Equations (48), (59), (61) and (65) result in closed ODE (7) for a, which is the first main result of this paper. Figure 4 shows $\partial_\tau a$ as a function of a for RKSE simulations with different initial conditions (the same initial conditions as in figure 1). Notice that after an initial transient all curves collapse to the single curve given by equation (7). This suggests that we can use the proximity of numerical curves to the analytical curve as the criterion for selecting t_0 in equation (10). In figure 1, we used the values of t_0 defined for each initial condition as the time $t = t_0$ when the relative difference between numerical and analytical curves reduces down to 20%. Arrows in figure 4 point to locations $(a(t_0), \partial_\tau a(t_0))$ satisfying this criterion. Table 1 shows the numerical values of parameters $\tau(t_0)$, t_0, t_c, L_0, a_0 and $\partial_\tau a(t_0)$ extracted from RKSE simulations (correspond to the simulations shown by solid lines in figure 1). The procedure of the extraction of $L(t)$ from simulations is described in section 7.

The dashed curves in figure 1 are only weakly sensitive to the choice of $t_0 < t_c$, provided t_0 is chosen later than the time specified by the 20%-difference criterion. For instance, if we choose t_0 based on 10%-difference criterion (instead of 20%), the $L(t)$ curves in figure 1 would change by $<5\%$ which is within the relative error of these curves in comparison with the numerics (solid curves in figure 1).

It also follows from equations (53), (58), (60) and (63) that the expansion coefficients in (44) are given by the following expressions:

$$\begin{aligned} c_1 &= \frac{1}{2} - \frac{1}{2\ln\frac{1}{a}} + \frac{1}{2}(-2 + 4d_2^{(1)} - \gamma + \ln 2)\frac{1}{(\ln\frac{1}{a})^2} + O\left(\frac{1}{(\ln\frac{1}{a})^3}\right), \\ c_2 &= -\frac{1}{2} + \frac{d_2^{(1)}}{\ln\frac{1}{a}} + O\left(\frac{1}{(\ln\frac{1}{a})^2}\right), \\ c_3 &= \frac{1}{2(\ln\frac{1}{a})^2} + O\left(\frac{1}{(\ln\frac{1}{a})^3}\right). \end{aligned} \tag{66}$$

Thus, the coefficient c_3, which corresponds to positive eigenvalue, is of a lower order compare with c_1 and c_2. We expect the similar to be true for all coefficients $c_3, c_4, \ldots$. Also, the coefficient $d_2^{(1)}$ is undetermined in our approximation order. We expect that it might depend on initial conditions. We conclude that the self-similar solution (29) is stable with respect to

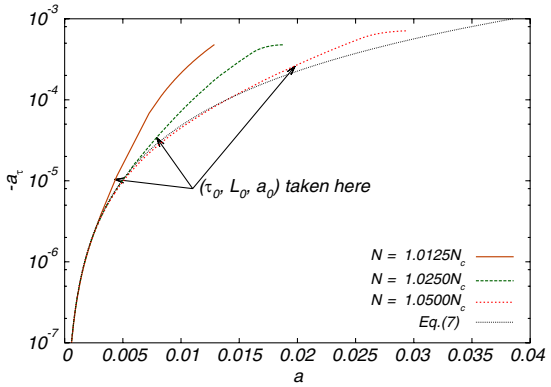

Figure 4. Dependence $\partial_\tau a(a)$ extracted from RKSE simulations shown in figure 1 (thick solid, dashed and short-dashed lines, respectively). The thin dotted line represents the analytical dependence $\partial_\tau a(a)$ from equation (7), with neglected $O(\ldots)$ term. Notice that after the initial transient all numerical curves collapse on the analytical curve. The arrows point to the locations where the relative difference between the analytical and numerical curves reduces to 20%. These locations define $\tau(t_0)$, t_0, L_0, a_0 and $\partial_\tau a(t_0)$ with the numerical values given in table 1.

radially symmetric perturbations, and the leading-order corrections to it are determined by a linear combination $v \simeq c_1\psi_1 + c_2\psi_2$, where c_1 and c_2 are given by (66).

6. Blow-up rate of self-similar solution

In this section we solve ODE (7) together with (8) and (9) to derive the blow-up rate (3). Integration of equation (7) from an initial value τ_0 to τ gives

$$\frac{1}{a}\left[\ln\frac{1}{a} + \tilde{M} + \frac{b}{\ln\frac{1}{a}} + O\left(\frac{1}{(\ln\frac{1}{a})^2}\right)\right]\Bigg|_{\tau=\tau_0}^{\tau} = 2(\tau - \tau_0), \tag{67}$$

where $\tilde{M} = M/2 - 1 = -2 - \gamma + \ln 2$ and $b = b_0/2 + M^2/4 = 1 + \pi^2/6$ as in (10). If we look at equation (67) as the implicit expression to determine $a(\tau)$ then it turns into a remote relative of the Lambert W-function. Such implicit expression can be solved for a assuming $\tau \gg 1$ by iterations as follows:

$$\ln\frac{1}{a} = L_1 - L_2 + \frac{L_2}{L_1} + \frac{L_2^2}{2L_1^2} - \frac{L_2}{L_1^2} - \frac{\tilde{M}}{L_1} + \frac{-2b + 2\tilde{M} + \tilde{M}^2 - 2\tilde{M}L_2}{2L_1^2} + O\left(\frac{L_2^3}{L_1^3}\right), \tag{68}$$

where $L_1 := \ln[2(\tau - \tau^*)]$, $L_2 := \ln\ln[2(\tau - \tau^*)]$, and

$$\tau^* = \tau_0 - \frac{1}{2a}\left(\ln\frac{1}{a} + \tilde{M} + \frac{b}{\ln\frac{1}{a}}\right)\Bigg|_{a=a_0}, \qquad a_0 = a(\tau_0). \tag{69}$$

At this point, one can proceed in qualitatively similar way to [14] to determine $L(\tau)$. However that way of calculation results in a slow convergence of the asymptotic series for $L(\tau)$ with the increase of τ. We choose a different path. Our goal is to start with equation (67), to carry as many steps of exact transformations as possible, and to perform asymptotic expansions as late as possible. Here and below we abuse notation and use the same notations for all functions with the same physical meaning, independently of their arguments: $L = L(t) = L(\tau) = L(a)$, $\tau = \tau(t) = \tau(L) = \tau(a)$ and $a = a(t) = a(\tau) = a(L)$. Similar, for initial values $L_0 = L(t_0) = L(\tau_0) = L(a_0)$, $\tau_0 = \tau(t_0) = \tau(L_0) = \tau(a_0)$ and $a_0 = a(t_0) = a(\tau_0) = a(L_0)$.

We use equations (8) and (9) to express a through τ-derivative of L as follows:

$$a = -\frac{\partial_\tau L}{L}. \tag{70}$$

We integrate (70) in τ between τ_0 and τ, using the integration by parts, to obtain

$$\begin{aligned} -\ln\frac{L}{L_0} &= \int_{\tau_0}^{\tau} a(\tau)\,\mathrm{d}\tau = a\tau(a) - a_0\tau(a_0) - \int_{a_0}^{a} \tau\,\mathrm{d}a \\ &= \left[\tau - \tau^*\right]a - \left[\tau_0 - \tau^*\right]a_0 - \int_{a_0}^{a} (\tau - \tau^*)\,\mathrm{d}a. \end{aligned} \tag{71}$$

To evaluate integral over a in (71) explicitly we use $\tau(a)$ from (67) with (69) and obtain

$$\begin{aligned} -\ln\frac{L}{L_0} &= \frac{1}{4}\left[\left(\ln\frac{1}{a}\right)^2 - \left(\ln\frac{1}{a_0}\right)^2\right] + \frac{\tilde{M}+1}{2}\left(\ln\frac{1}{a} - \ln\frac{1}{a_0}\right) \\ &\quad + \frac{b}{2}\left(\ln\ln\frac{1}{a} - \ln\ln\frac{1}{a_0}\right) + \frac{b}{2}\left(\frac{1}{\ln\frac{1}{a}} - \frac{1}{\ln\frac{1}{a_0}}\right) + O\left(\frac{1}{\ln\frac{1}{a}}\right). \end{aligned} \tag{72}$$

Note also that the term $O(\frac{1}{\ln\frac{1}{a}})$ in (72) originates from the next order term $O(\frac{1}{(\ln\frac{1}{a})^2})$ in equation (67). Formally, in equation (72), the terms $O(\frac{1}{\ln\frac{1}{a}})$ and $\frac{b}{2\ln\frac{1}{a}}$ are of the same order. Yet, our numerical simulations indicate that $\frac{b}{2\ln\frac{1}{a}}$ term improves accuracy of the analytic approximation, so we keep this term in its explicit form.

We introduce new variables,

$$l := \ln\frac{1}{L} \qquad \text{and} \qquad l_0 := \ln\frac{1}{L_0}, \tag{73}$$

as well as define

$$l^* = l_0 - \frac{1}{4}\left(\ln\frac{1}{a_0}\right)^2 - \frac{\tilde{M}+1}{2}\ln\frac{1}{a_0} - \frac{b}{2}\left(\ln\ln\frac{1}{a_0} + \frac{1}{\ln\frac{1}{a_0}}\right), \tag{74}$$

which allows to rewrite (72) as follows:

$$l - l^* = \frac{1}{4}\left(\ln\frac{1}{a}\right)^2 + \frac{\tilde{M}+1}{2}\ln\frac{1}{a} + \frac{b}{2}\left(\ln\ln\frac{1}{a} + \frac{1}{\ln\frac{1}{a}}\right) + O\left(\frac{1}{\ln\frac{1}{a}}\right). \tag{75}$$

We now solve equation (75) for $\ln\frac{1}{a}$. Instead of doing straightforward iterations, we neglect the terms $\frac{b}{2}(\ldots)$, $O(\frac{1}{\ln\frac{1}{a}})$ in equation (75) and solve the remaining part of the equation, $Y_0^2 - 2Y_0 - V = 0$, exactly:

$$Y_0 = 1 + \sqrt{1+V}, \tag{76}$$

where we define

$$Y := -\frac{\ln\frac{1}{a}}{\tilde{M}+1} \qquad \text{and} \qquad V := \frac{4}{(\tilde{M}+1)^2}(l - l^*) \tag{77}$$

with Y_0 being the leading-order approximation to Y, such that

$$Y = Y_0 + \delta Y. \tag{78}$$

To find δY as a function of V, we represent δY through the formal series $\delta Y = \sum_{n=1}^{\infty} \delta Y_{-n}/Y_0^n$ (with Y_0 given by (76)). We use this series together with (76)–(78) to perform a series expansion of equation (75) in inverse powers of Y_0. It allows to determine the coefficients

δY_n recursively at integer inverse powers of Y_0 starting with the power zero. In particular, the zero power gives $Y_{-1} = -b\ln[-(1+\tilde{M})Y_0]/(1+\tilde{M})^2$. Note that the double logarithm $\ln\ln\frac{1}{a}$ in (75) also needs to be expanded. All together it results in

$$\delta Y = -\frac{b\ln\left[-(1+\tilde{M})Y_0\right]}{(1+\tilde{M})^2 Y_0} + \frac{-b(1+\tilde{M})\ln\left[-(1+\tilde{M})Y_0\right]+b}{(1+\tilde{M})^3 Y_0^2} + O\left(\frac{1}{Y_0^2}\right) + O\left(\frac{(\ln Y_0)^2}{Y_0^3}\right). \tag{79}$$

Here, similar to (72), we keep the term $b/(1+\tilde{M})^3 Y_0^2$, even though this term is of the same order as $O(1/Y_0^2)$ term. Here, $\tilde{M}+1 = -0.884\,068\ldots$ according to (10). Note, that instead of performing an expansion in inverse powers of Y_0, one can simply do it in inverse powers of $V^{1/2}$. This, however, would result in a slower convergence for moderate ($V \gtrsim 1$) values of V.

We rewrite (8) as $-(L\,\mathrm{d}L/a) = \mathrm{d}t$, and integrate it between time t_c and t:

$$\int_t^{t_c} \mathrm{d}t' = t_c - t = -\int_L^0 \frac{L'}{a(L')}\,\mathrm{d}L', \tag{80}$$

where following (73) and (77) we can represent L through V as $L = \exp\left(-[l^* + ((\tilde{M}+1)^2/4)V]\right)$. The dependence $a(L)$ in (80) follows from (73)–(79). Switching from integration over L to the integration over Y_0 in (80) we obtain:

$$\begin{aligned} t_c - t = \int_{Y_0}^{\infty} &\exp\left(-2\left[l^* + \frac{(\tilde{M}+1)^2}{4}[(Y_0'-1)^2-1]\right]\right)\frac{(\tilde{M}+1)^2}{2}(Y_0'-1) \\ &\times \exp\left(-(1+\tilde{M})Y_0' + \frac{b\ln\left[-(1+\tilde{M})Y_0'\right]}{(1+\tilde{M})Y_0'}\right. \\ &\left. -\frac{-b(1+\tilde{M})\ln\left[-(1+\tilde{M})Y_0'\right]+b}{(1+\tilde{M})^2 Y_0'^2} + O\left(\frac{1}{Y_0'^2}\right)\right)\mathrm{d}Y_0'. \end{aligned} \tag{81}$$

Here, the integration cannot be carried explicitly. Instead, we use the Laplace method (see e.g. [48, 49]) to evaluate the integral asymptotically in the limit $Y_0 \gg 1$. We introduce in equation (10) a new integration variable,

$$z := Y_0' - Y_0, \tag{82}$$

and rewrite equation (81) as

$$t_c - t = \frac{(\tilde{M}+1)^2}{2}\exp\left[-2l^* - \frac{(\tilde{M}+1)^2}{2}Y_0^2 + (\tilde{M}+1)\tilde{M}Y_0\right]\int_0^{\infty} \mathrm{e}^{Y_0 S(z,Y_0)}\,\mathrm{d}z, \tag{83}$$

where

$$\begin{aligned} S(z,Y_0) = &-(\tilde{M}+1)^2 z + \frac{1}{Y_0}\left[-\frac{(\tilde{M}+1)^2}{2}z^2 + (\tilde{M}+1)\tilde{M}z + \ln(Y_0+z-1)\right] \\ &+ \frac{b\ln\left[-(1+\tilde{M})(Y_0+z)\right]}{Y_0(1+\tilde{M})(Y_0+z)} - \frac{-b(1+\tilde{M})\ln\left[-(1+\tilde{M})(Y_0+z)\right]+b}{Y_0(1+\tilde{M})^2(Y_0+z)^2} \\ &+ O\left(\frac{1}{Y_0(Y_0+z)^2}\right). \end{aligned} \tag{84}$$

To use the Laplace method for asymptotic expansion of the integral in (83), we start with the following general expression, [48, 49]:

$$\int_0^\infty \mathrm{e}^{Y_0 S(z,Y_0)}\,\mathrm{d}z = \mathrm{e}^{Y_0 S(0,Y_0)} \sum_{n=0}^{\infty} c_n Y_0^{-n-1} \tag{85}$$

with

$$c_n = (-1)^{n+1}\left(\frac{1}{S'(z,Y_0)}\frac{\partial}{\partial z}\right)^n \left(\frac{1}{S'(z,Y_0)}\right)\Bigg|_{z=0}, \qquad S'(z,Y_0) := \frac{\partial}{\partial z} S(z,Y_0). \tag{86}$$

Taking into account two leading terms in (85), we obtain from (83), (84), (85), and (86) the following expression:

$$\begin{aligned} t_\mathrm{c} - t = {} & \frac{(\tilde{M}+1)^2}{2} \exp\left[-2l^* - \frac{(\tilde{M}+1)^2}{2} Y_0^2 + (\tilde{M}+1)\tilde{M} Y_0 + \ln(Y_0 - 1)\right] \\ & \times \exp\left[\frac{b \ln\left[-(1+\tilde{M})Y_0\right]}{(1+\tilde{M})Y_0} - \frac{-b(1+\tilde{M})\ln\left[-(1+\tilde{M})Y_0\right] + b}{(1+\tilde{M})^2 Y_0^2} + O\left(\frac{1}{Y_0^2}\right)\right] \\ & \times \frac{1}{(\tilde{M}+1)^2 Y_0}\left[1 + \frac{\tilde{M}}{(1+\tilde{M})Y_0} + \frac{\tilde{M}^2}{(1+\tilde{M})^2 Y_0^2} + O\left(\frac{\ln Y_0}{Y_0^3}\right)\right]. \end{aligned} \tag{87}$$

We now define a large parameter

$$x := \sqrt{-2\ln \beta (t_\mathrm{c} - t)} - \tilde{M}, \tag{88}$$

where

$$\beta := 2\exp\left\{2l^* - \frac{\tilde{M}^2}{2}\right\}. \tag{89}$$

We multiply both the lhs and the rhs of (87) by β from (89) and take logarithm from both sides to obtain $-x^2/2$ on the lhs. We solve the resulting equation for Y_0 by assuming the asymptotic form,

$$Y_0 = b_{-1} x + \sum_{n=0}^{\infty} \frac{b_n}{x^n}. \tag{90}$$

and performing a series expansion of both rhs and lhs of that resulting equation in inverse powers of x. The coefficients b_{-1}, , $b_1, \ldots,$ b_3 are determined recursively giving

$$\begin{aligned} Y_0 = {} & -\frac{1}{\tilde{M}+1}\left[x + \frac{1 - b\ln x}{x^2} + \frac{-\frac{1}{2} - 2\tilde{M} + b(\ln x + 2\tilde{M}\ln x - 1)}{x^3}\right] \\ & + O\left(\frac{1}{x^3}\right) + O\left(\frac{(\ln x)^2}{x^4}\right). \end{aligned} \tag{91}$$

Note that the choice of the factor $\exp\{-\tilde{M}^2/2\}$ in (89) is somewhat arbitrary (the lhs and the rhs of (87) can be multiplied by an arbitrary positive constant). The factor $\exp\{-\tilde{M}^2/2\}$ is chosen to speed up convergence of (91) for $Y_0 \gtrsim 1$, i.e. for $L(t) \lesssim 1$.

Using (73), (76) and (77) we obtain

$$L(t) = \exp\left[-l^* - \frac{(\tilde{M}+1)^2}{4}(Y_0^2 - 2Y_0)\right]. \tag{92}$$

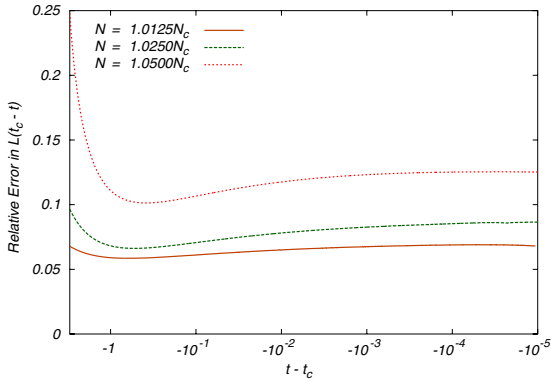

Figure 5. The absolute value of the relative error between $L(t)$ from RKSE simulations and the scaling (10). The results of the same simulations as in figure 1(*c*) are used as well as the data of table 1.

Equations (73), (74) (88), (89), (91) and (92) give the closed expression for $L(t)$ as a function of $t_c - t$ and the initial values $L_0 = L(t_0)$, $a_0 = -LL_t|_{t=t_0}$. To make the comparison with the old scaling (6) more transparent, we plug the expression for Y_0 from (91) into (92) and perform a series expansion of the expression in the exponent into inverse powers of x, obtaining the final expression (10). Note that the first term in the exponent of the first equation in (10) can be rewritten through x as $-\sqrt{-(\ln \beta(t_c - t))/2} = -((x + \tilde{M})/2)$. Thus, equation (10) includes terms of orders x and x^0.

The error terms $O(1/x^3)$ in (91) and $O(1/x^2)$ in (10) result from the error term $O(1/(\ln \frac{1}{a})^4)$ in equation (7). We, however, chose to write down explicitly the terms of the same orders, $\propto \frac{1}{x^3}$ in (91) and $\propto \frac{1}{x^2}$ in (10). These terms are independent from the error term $O(1/(\ln \frac{1}{a})^4)$ of equation (7). Next order error terms are $O((\ln x)^2/x^4)$ in (91) and $O((\ln x)^2/x^3)$ in (10).

Comparison of the dependence $L(t)$ from the simulations of RKSE, the analytical expressions (5) and (10) are given in figure 1. The initial conditions for the scalings (5) and (10) are given in table 1. Figure 5 shows the absolute value of the relative error between $L(t)$ obtained from from RKSE simulations and the scaling (10) with all orders of x taken into account in (10). It is seen that the relative error decreases with the decrease of N. For smaller values $t_c - t < 10^{-16}$ we do not have the results of RKSE simulations. Instead, figure 6 shows the absolute value of the relative error between $L(t)$ obtained from (5) and (10). It gives the estimate of the accuracy of the standard scaling (5). It is seen that (5) is asymptotically correct, but converges to (10) very slowly for unrealistically small values of L.

7. Numerical simulations of RKSE

In our numerical simulation we evolve equation (27), written in terms of the mass of bacteria $m(r, t)$ within the circle of radius r as defined in (26). The density, $\rho(r, t) = (1/r)(\partial m/\partial r)$, and other quantities characterizing the evolution of the collapse are computed from the mass. To find the width of the collapse, we assume that the solution has reached its self-similar form given by equation (25). Then, the collapse width can be estimated from the density at the center as $L = (\frac{1}{8}\rho|_{r=0})^{-1/2}$. To compute the slow parameter, a, we differentiate $L(t)$, as in (8). The self-similar time, τ, is found by integrating $L(t)$ according to equation (9).

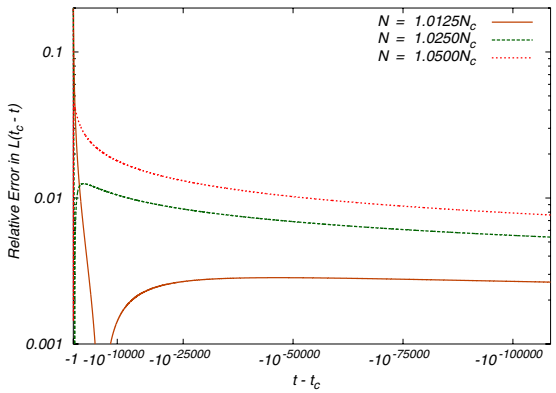

Figure 6. The absolute value of the relative error between the scalings (5) and (10). The data of table 1 are used for both scalings.

A typical solution for $m(r, t)$ is shown in figure 3(b). The spatial extent of the collapse is marked by the large gradient of the solution near the center, which becomes even larger and moves even closer to the center as time progresses. This requires special treatment to ensure that the solution remains well-resolved.

The results presented in this paper are obtained using an adaptive mesh refinement (AMR) technique [32, 50], complemented with the fourth-order Runge–Kutta time advancement method. Our spatial domain, $r \in [0, r_{\max}]$, is divided into several subdomains (subgrids) with different spatial resolution. The spacing between computational points is constant for each subgrid, and differs by a factor of two between adjacent subgrids. The rightmost subgrid, farthest from the collapse, has the coarsest resolution; the spatial step decreases in the inward direction.

The grid structure adapts during the evolution of the collapse to keep the solution well resolved. When a refinement condition is met, the leftmost subgrid is divided in two equal subgrids. Then, the new leftmost subgrid is refined; that is, additional computational points are placed halfway between the existing points. The values at the new points are obtained with sixth-order interpolation. The condition for grid refinement comes naturally from properties of the self-similar profile. The density at the origin increases by a factor of 4 as the width of profile decreases by a factor of 2 according to equation (3). To keep the effective number of grid points per L within desired limits, we use the increase of the maximum density by factor of 4 as the condition for refinement.

In the interior of each subgrid, the spatial derivatives are computed using fourh-order central differences on the five point stencil. At the subgrid boundaries, the data are copied between subgrids to fill in values at 'ghost points', as shown by arrows in figure 7. Notice that communication between subgrids is going in both directions: in AMR terminology, data from the fine subgrid is restricted to the coarse grid ghost points, and data from the coarse grid is prolongated to the fine grid ghost points. The data between points of the coarser subgrids needed for finer subgrid ghost points are obtained by sixth-order interpolation. The left ghost points of the leftmost subgrid are filled using reflective boundary conditions. The point $r = 0$ is treated in a special way because of the singularity in the rhs of equation (27). Expanding $m(r, t)$ in a power series in r at the origin and using the definition (26) we obtain that $m(r, t) = (\rho(0, t)r^2/2) + O(r^4)$. This is also consistent with the series expansion in r of rhs of equation (27). Thus in the spatial discretization we set $m(r = 0, t) = 0$. The right

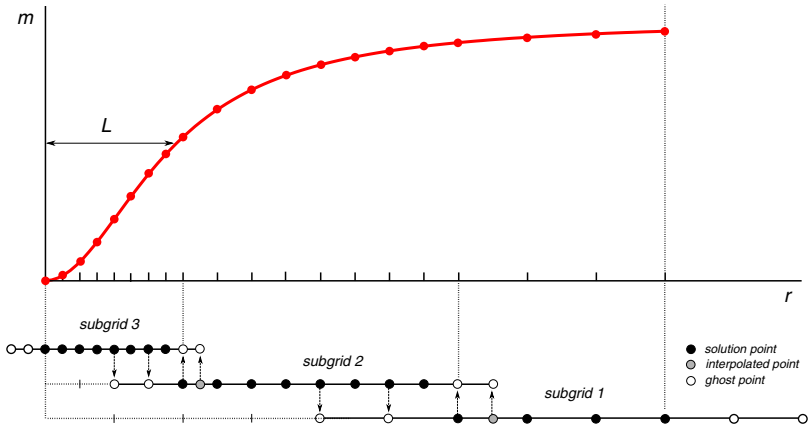

Figure 7. Schematic representation of the discretized solution and the grid structure. Three subgrids are shown. The subgrids closer to the center of the collapse have finer resolution. The data at black points are evolved by the discretized equation (27), the data at white points are copied from neighboring subgrids (the copying is shown by arrows), the data in gray points are interpolated from neighboring points using sixth-order polynomial.

ghost points of the rightmost subgrid are filled with the data from the last point. We found the right boundary conditions to be very forgiving, which is not surprising considering that the mass approaches a constant, as r^{-3}, when $r \to \infty$.

The solution on all subgrids is evolved with the same timestep, $\Delta t = C_{\rm CFL} h^2$, where h is the spatial step of the finest grid and $C_{\rm CFL}$ is the constant. We typically used $C_{\rm CFL} = 0.4$ but also tested a convergence for smaller values of $C_{\rm CFL}$.

We use two kinds of initial conditions. First kind is the Gaussian,

$$m|_{t=0} = A\left(1 - \mathrm{e}^{-(r/\sigma)^2}\right),$$

which implies

$$\rho|_{t=0} = \frac{2A}{\sigma^2}\mathrm{e}^{-(r/\sigma)^2},$$

where σ and A are the parameters of the initial condition. Second kind is the modified stationary solution, $m|_{t=0} = Am_0(r)$, where $m_0(r)$ is given by equation (28). Both types of initial data result in similar dynamics for the same values of $N = 2\pi A$. The simulations presented in this paper were performed for Gaussian initial conditions, with $\sigma = 1$ and $A = 4.05$, 4.1 and 4.2. The initial grid was comprised of ten subgrids; the finest subgrid had 400 points while all other subgrids had 200 points each. The size of domain was set to $r_{\rm max} = 1600 L_0$.

We have verified the AMR code against an independently developed, uniform-grid code with an adaptive spatial resolution and an adaptive time step. Similar to the AMR code, the uniform-grid code evolved equation (27) using fourth-order Runger–Kutta integration in time. The spatial derivatives were computed spectrally using the `FFTW-3` library [51]. Since Fourier transforms require periodic boundary conditions, the spatial domain was extended to $r \in [-r_{\rm max}, r_{\rm max}]$ with sufficiently large $r_{\rm max}$ (about $50L_0$). As in the AMR code, we set the value of the mass to zero at the origin point to avoid the singularity in the rhs of the equation. Although uniform in space, the grid resolution was refined at times when the maximum density increases by a factor of four. The new grid had twice as many points with values computed by spectral interpolation. We run the uniform-grid code at $C_{\rm CFL} = 0.2$.

Although the uniform-grid code was useful for cross-comparison, it was significantly less efficient than the AMR code. Typically, we run the uniform-grid code until the peak density reached $\approx 10^5$, which required 32 768 gridpoints with grid resolution $(L/8) < h < (L/4)$. On the other hand, in the AMR simulations presented here, the density reached $\approx 10^{17}$ on approximately 12 000 total gridpoints, with $(L/100) < h < (L/50)$ resolution on the finest subgrid.

8. Conclusion and discussion

In conclusion, we studied the collapsing solution of the 2D RKSE, equation (1). To leading order, the collapsing solution has the self-similar form (3), characterized by the scaling $L(t)$. Our analysis of the dynamics of perturbations about the self-similar form allowed us to find the time dependence of the width of the collapsing solution given by the scaling (10). The analysis of the perturbations is performed by switching to independent 'blow-up' variables (30), and an unknown function (31). In the blow-up variables, the analysis of the dynamics of the collapse reduces to the analysis of the perturbation about the static solution (29). The analysis exploits the slow evolution of the parameter a, defined in (8), which originates from the leading-order scaling $L(t) \propto (t_c - t)^{1/2}$. After applying the gauge transform (33), we expanded the general perturbations in eigenfunctions of the self-adjoint linearization operator $\hat{\mathcal{L}}_a$ about the static solution and derived the system of amplitude equations. We solved these amplitude equations approximately to obtain ODE (7) for $a(\tau)$. We solve equation (7) asymptotically in the limit $t \to t_c$, together with (8) and (9) to obtain the scaling (10).

We found that both ODE (7) for $a(\tau)$ and the scaling (10) for $L(t)$ are in excellent agreement with numerical simulations of RKSE. We compared the scaling (10) with the previously known scalings (4)–(6) and showed that scaling (5) is the correct asymptotic limit. However, this limit dominates only for unrealistically small values (see the expressions (11) and (12) for the typical numerical estimates of these small values). In contrast, the scaling (10) agrees well with simulations for a quite moderate decrease of $L(t)$ compared to the initial condition. E.g., figure 2 shows that six-fold decrease of L compare with the initial value $L(0)$ is enough to achieve the relative error $\lesssim 7\%$ between simulations and the scaling (10).

We now discuss the limitations of the analysis of this paper. The analysis is exact until we derive the amplitude equation (46). At this point we must resort to approximation, because we can calculate only a finite number of terms in the amplitude equation. We approximate the eigenfunctions ψ_j of $\hat{\mathcal{L}}_a$ as $\tilde{\psi}_j$, $j = 1, 2, \ldots$ through the variational analysis (see section 4). Such variational approximation itself does not create any obstacle because one can, at least in principle, expand the general perturbation about the static solution in functions $\tilde{\psi}_j$, provided they form a complete set on the space $L^2([0, \infty), y^3\,\mathrm{d}y)$ which corresponds to the scalar product (38). However, the variational construction of such functions turns out to be difficult for $j > 3$ (provided we aim to approximate the eigenvalues λ_j of $\hat{\mathcal{L}}_a$ with high precision). This work is left for the future. In this paper we limit the analysis of the amplitude equations for $\tilde{\psi}_j$, $j = 1, 2, 3$ by setting $c_j = 0$ for $j > 3$ in the amplitude equation. We found that already $\tilde{\psi}_3$ gives contribution only to the coefficient b_0 in ODE (7), i.e. to the highest order term $b_0/(\ln \frac{1}{a})^3$ which we take into account. The other two lower order terms in rhs of (7), $-(2/\ln \frac{1}{a}) + M/(\ln \frac{1}{a})^2$, are fully determined by $\tilde{\psi}_1$ and $\tilde{\psi}_2$. We expect that taking into account the non-zero values of $\tilde{\psi}_j$ and c_j for $j > 3$ might modify the value of b_0 in ODE for $a(\tau)$ (and respectively modify b in (10)). Such type of calculation presents a technical challenge and is left for the future. A potential route for such calculation might be the approximation of the eigenfunctions ψ_j using the matched asymptotic technique [15]. Using this technique,

however, one faces the challenge of calculating the scalar products in the amplitude equation. It should be mentioned that the dramatic improvement of the accuracy of $L(t)$ with the increase of the order of approximation (as seen in comparison of figures 1(b), (c) with figure 1(a)) suggests that the essential part of b_0 (and respectively b) is already captured in our scaling (10).

Appendix A. Keller–Segel model of bacterial aggregation

Bacteria and biological cells often communicate through chemotaxis, the process of secretion and detection of a substance called chemoattractant. Below we refer to bacteria and cell as synonyms. The chemoattractant secreted by bacteria diffuses through media. Other bacteria of the same kind detect it and move along its gradient. Thus the chemotaxis creates non-local attraction between bacteria. Bacteria are self-propelled and, without the chemotactic clue, the center of mass of each bacterium typically experiences a random walk. The motion of bacterial colonies is thus affected by the competition between random-walk-based diffusion and chemotaxis-based attraction. The macroscopically averaged motion of bacteria can be described by the Keller–Segel model (sometimes called the Patlak–Keller–Segel equation), see e.g., [1–16] and references therein:

$$\partial_t \rho = D\nabla^2 \rho - \nabla\big[k\rho\, \nabla c\big], \tag{A.1}$$

$$\partial_t c = D_c \nabla^2 c + \alpha\, \rho, \tag{A.2}$$

where $\rho(\boldsymbol{r}, t)$ is the bacterial density at spatial point $\boldsymbol{r}$ and time t, $c(\boldsymbol{r}, t)$ is the concentration of chemoattractant, D is the diffusion coefficient of bacteria (representing the random walk), D_c is the diffusion coefficient of chemoattractant, α is the production rate of chemoattractant by bacteria, and the coefficient $k > 0$ characterizes the strength of chemotaxis.

The Keller–Segel model is a mean-field approximation of the behaviour of a large number of bacteria, and can be derived from the dynamics of individual bacteria using macroscopic averaging over an ensemble of realizations of stochastic bacteria motion. A starting point of the derivation can be, e.g., the description of an ensemble of bacteria as point-wise objects subject to a white noise force, as in [13]. Such description is most relevant to procaryotic bacteria like *Escherichia coli* which small rigid shapes. Another possible starting point is the description of the dynamics of eukaryotic organisms with randomly fluctuating shape, such as *Dictyostelium* amoeba [24–26].

If the initial density of bacteria is low, the bacterial diffusion typically dominates attraction and the density remains low. For instance, a typical time scale for the evolution of a low-density *Escherichia coli* distribution in a petri dish is about one day [5] (see figure 3(A) in [5]). If the initial density is relatively high, attraction dominates, and bacteria aggregate (see figure 3B in reference [5]). The typical time scale of such aggregation in experiments on *Escherichia coli* is several minutes [5]. Thus the aggregation has an explosive character compared to the evolution of bacteria outside the aggregation area. The aggregation is described by the 'collapse of bacterial density' in the approximation of the Keller–Segel model (A.1)–(A.2).

The diffusion of chemoattractant is usually much faster than the diffusion of bacteria, i.e. $D/D_c \ll 1$. For instance, $D/D_c \sim 1/40 - 1/400$ for the cellular slime mold *Dictyostelium* [52], and $D/D_c \sim 1/30$ for microglia cells and neutrophils [53, 54]. (Here, we refer to bacteria and cell as synonyms.) Thus equation (A.2) evolves on a much smaller time scale than equation (A.1), so we can neglect the time derivative in (A.2). In addition, we assume that D, D_c, α, and k are constants, and recast all variables in dimensionless form: $t \to t_0 t$, $r \to t_0^{1/2} D^{1/2} r$, $\rho \to (D_c/t_0 \alpha k)\rho$, and $c \to (D/k)c$, where t_0 is a typical timescale of the dynamics of ρ in equation (A.1). The resulting system is called the reduced Keller–Segel equations (1).

Appendix B. Calculation of scalar products through Meijer G-function and Γ-function

Calculation of scalar products in section 5 requires to evaluate the integrals of the following type:

$$I_l^{n,m} := \int_0^\infty \frac{\mathrm{e}^{-\frac{a}{2}y^2} y^{2n+1} [\ln(1+y^2)]^m}{(1+y^2)^l}\,\mathrm{d}y, \quad n,m,l \in \mathbb{N}, \qquad n \geqslant 0, l \geqslant 2, m \geqslant 0, \tag{B.1}$$

which by the change of variable $x := 1 + y^2$ and differentiation over the parameter a reduces to the following expression

$$\begin{aligned} I_l^{n,m} &= (-1)^n 2^{n-1} \frac{\mathrm{d}^n}{\mathrm{d}a^n} \int_1^\infty \frac{\mathrm{e}^{-\frac{a}{2}(x-1)} [\ln x]^m}{x^l}\,\mathrm{d}x \\ &= (-1)^n 2^{n-1} m! \frac{\mathrm{d}^n}{\mathrm{d}a^n} \left[\mathrm{e}^{\frac{a}{2}} G^{m+2,0}_{m+1,m+2}\left(\frac{a}{2} \middle| \begin{matrix} l, \ldots, l \\ 0, l-1, \ldots, l-1 \end{matrix} \right) \right], \end{aligned} \tag{B.2}$$

where $G^{l,k}_{p,q}\left(z \middle| \begin{matrix} a_1, \ldots, a_p \\ b_1, \ldots, b_q \end{matrix} \right)$ is the Meijer G-function [55, 56].

E.g., for $n = 0$ and $l = 2$:

$$\begin{aligned} I_2^{0,1} &= \frac{1}{2}\mathrm{e}^{\frac{a}{2}} G^{3,0}_{2,3}\left(\frac{a}{2} \middle| \begin{matrix} 2, 2 \\ 0, 1, 1 \end{matrix} \right), \\ I_2^{0,2} &= \mathrm{e}^{\frac{a}{2}} G^{4,0}_{3,4}\left(\frac{a}{2} \middle| \begin{matrix} 2, 2, 2 \\ 0, 1, 1, 1 \end{matrix} \right), \\ I_2^{0,3} &= 3\mathrm{e}^{\frac{a}{2}} G^{5,0}_{4,5}\left(\frac{a}{2} \middle| \begin{matrix} 2, 2, 2, 2 \\ 0, 1, 1, 1, 1 \end{matrix} \right), \\ I_2^{0,4} &= 12\mathrm{e}^{\frac{a}{2}} G^{6,0}_{5,6}\left(\frac{a}{2} \middle| \begin{matrix} 2, 2, 2, 2, 2 \\ 0, 1, 1, 1, 1, 1 \end{matrix} \right). \end{aligned} \tag{B.3}$$

And more generally, for $n = 0$ and $l \geqslant 2$:

$$\begin{aligned} I_l^{0,1} &= \frac{1}{2}\mathrm{e}^{\frac{a}{2}} G^{3,0}_{2,3}\left(\frac{a}{2} \middle| \begin{matrix} l, l \\ 0, l-1, l-1 \end{matrix} \right), \\ I_l^{0,2} &= \mathrm{e}^{\frac{a}{2}} G^{4,0}_{3,4}\left(\frac{a}{2} \middle| \begin{matrix} l, l, l \\ 0, l-1, l-1, l-1 \end{matrix} \right), \\ I_l^{0,3} &= 3\mathrm{e}^{\frac{a}{2}} G^{5,0}_{4,5}\left(\frac{a}{2} \middle| \begin{matrix} l, l, l, l \\ 0, l-1, l-1, l-1, l-1 \end{matrix} \right), \\ I_l^{0,4} &= 12\mathrm{e}^{\frac{a}{2}} G^{6,0}_{5,6}\left(\frac{a}{2} \middle| \begin{matrix} l, l, l, l, l \\ 0, l-1, l-1, l-1, l-1, l-1 \end{matrix} \right). \end{aligned} \tag{B.4}$$

A particular case $m = 0$ is especially easy because the G-function from (B.1) reduces to the incomplete Gamma function $\Gamma(s, z) = \int_z^\infty t^{s-1}\mathrm{e}^{-t}\,\mathrm{d}t$ as follows:

$$I_l^{n,0} = (-1)^n 2^{n-l} a^{l-1} \frac{\mathrm{d}^n}{\mathrm{d}a^n} \left[\mathrm{e}^{\frac{a}{2}} \Gamma\left(1-l, \frac{a}{2}\right) \right]. \tag{B.5}$$

A Taylor series expansion of (B.5) for $a \to 0$ gives for $n = 0$ the following expressions:

$$
\begin{aligned}
I_2^{0,0} &= \tfrac{1}{2} + \tfrac{1}{4}(\gamma - \ln 2 + \ln a)a + \tfrac{1}{8}(-1 + \gamma - \ln 2 + \ln a)a^2 + O(a^3 \ln a),\\
I_3^{0,0} &= \frac{1}{4} - \frac{a}{8} + \frac{1}{16}(-\gamma + \ln 2 - \ln a)a^2 + \frac{1}{32}(1 - \gamma + \ln 2 - \ln a)a^3 + O(a^4 \ln a),\\
I_4^{0,0} &= \frac{1}{6} - \frac{a}{24} + \frac{a^2}{48} + \frac{1}{96}(\gamma - \ln 2 + \ln a)a^3 + \frac{1}{192}(-1 + \gamma - \ln 2 + \ln a)a^4\\
&\quad + O(a^5 \ln a),\\
I_5^{0,0} &= \frac{1}{8} - \frac{a}{48} + \frac{a^2}{192} - \frac{a^3}{384} + \frac{1}{768}(-\gamma + \ln 2 - \ln a)a^4 + \frac{(1 - \gamma + \ln 2 - \ln a)a^5}{1536}\\
&\quad + O(a^6 \ln a).
\end{aligned}
\tag{B.6}
$$

and the case $n > 0$ is obtained by the differentiation of these expressions according to (B.5).

A Taylor series expansion of (B.2) for $a \to 0$ gives for $n = 0$ the following expressions for $l = 1$:

$$
\begin{aligned}
I_2^{0,1} &= \tfrac{1}{2} + \tfrac{1}{48}(12\gamma - 6\gamma^2 - \pi^2 - 12\ln 2 + 12\gamma \ln 2 - 6(\ln 2)^2\\
&\quad + 12\ln a - 12\gamma \ln a + 12 \ln 2 \ln a - 6(\ln a)^2)a + \tfrac{1}{96}(12\gamma - 6\gamma^2 - \pi^2 - 12\ln 2\\
&\quad + 12\gamma \ln 2 - 6(\ln 2)^2 + 12\ln a - 12\gamma \ln a + 12 \ln 2 \ln a - 6(\ln a)^2)a^2 + O(a^3(\ln a)^2),\\
I_3^{0,1} &= \frac{1}{8} - \frac{3a}{16} + \frac{1}{192}\Big(- 18\gamma + 6\gamma^2 + \pi^2 + 18\ln 2 - 12\gamma \ln 2 + 6(\ln 2)^2 - 18\ln a + 12\gamma \ln a\\
&\quad - 12\ln 2 \ln a + 6(\ln a)^2\Big)a^2 + \frac{1}{384}\Big(6 - 18\gamma + 6\gamma^2 + \pi^2 + 18\ln 2 - 12\gamma \ln 2 + 6(\ln 2)^2\\
&\quad - 18\ln a + 12\gamma \ln a - 12\ln 2 \ln a + 6(\ln a)^2\Big)a^3 + O\left(a^4(\ln a)^2\right),\\
I_4^{0,1} &= \frac{1}{18} - \frac{5a}{144} + \frac{11a^2}{288} + \frac{1}{1152}\Big(22\gamma - 6\gamma^2 - \pi^2 - 22\ln 2 + 12\gamma \ln 2 - 6(\ln 2)^2 + 22\ln a\\
&\quad - 12\gamma \ln a + 12\ln 2 \ln a - 6(\ln a)^2\Big)a^3 + O\left(a^4(\ln a)^2\right),\\
I_5^{0,1} &= \frac{1}{32} - \frac{7a}{576} + \frac{13a^2}{2304} - \frac{25a^3}{4608}\\
&\quad + \frac{1}{9216}\Big(- 25\gamma + 6\gamma^2 + \pi^2 + 25\ln 2 - 12\gamma \ln 2 + 6(\ln 2)^2 - 25\ln a\\
&\quad + 12\gamma \ln a - 12\ln 2 \ln a + 6(\ln a)^2\Big)a^4 + O\left(a^5(\ln a)^2\right),
\end{aligned}
\tag{B.7}
$$

for $l = 2$:

$$
\begin{aligned}
I_2^{0,2} &= 1 + \Big[- \frac{1}{24}\left[-12 + 12\gamma - 6\gamma^2 - \pi^2 - 12\ln 2 + 12\gamma \ln 2 - 6(\ln 2)^2\right]\ln a\\
&\quad + \frac{1}{4}(-1 + \gamma - \ln 2)(\ln a)^2 + \frac{(\ln a)^3}{12}\Big]a + O(a) + O\left(a^2(\ln a)^3\right),\\
I_3^{0,2} &= \frac{1}{8} - \frac{7a}{16} + \Big[- \frac{1}{96}\left[21 - 18\gamma + 6\gamma^2 + \pi^2 + 18\ln 2 - 12\gamma \ln 2 + 6(\ln 2)^2\right]\ln a\\
&\quad + \frac{1}{32}(3 - 2\gamma + 2\ln 2)(\ln a)^2 - \frac{(\ln a)^3}{48}\Big]a^2 + O(a^2) + O\left(a^3(\ln a)^3\right),\\
I_4^{0,2} &= \frac{1}{27} - \frac{19a}{432} + \frac{85a^2}{864}\\
&\quad + \Big[- \frac{\left(-85 + 66\gamma - 18\gamma^2 - 3\pi^2 - 66\ln 2 + 36\gamma \ln 2 - 18(\ln 2)^2\right)\ln a}{1728}
\end{aligned}
$$

$$+\frac{1}{576}(-11+6\gamma-6\ln 2)(\ln a)^2+\frac{(\ln a)^3}{288}\Big]a^3+O(a^3)+O\left(a^4(\ln a)^3\right),$$

$$I_5^{0,2}=\frac{1}{64}-\frac{37a}{3456}+\frac{115a^2}{13824}-\frac{415a^3}{27648}$$
$$+\Big[-\frac{\left(415-300\gamma+72\gamma^2+12\pi^2+300\ln 2-144\gamma\ln 2+72(\ln 2)^2\right)\ln a}{55296}$$
$$+\frac{(25-12\gamma+12\ln 2)(\ln a)^2}{9216}-\frac{(\ln a)^3}{2304}\Big]a^4+O(a^4)+O\left(a^5(\ln a)^3\right), \tag{B.8}$$

and for $l=3$:

$$I_2^{0,3}=3+\Big[\frac{1}{16}\left(-12+12\gamma-6\gamma^2-\pi^2-12\ln 2+12\gamma\ln 2-6(\ln 2)^2\right)(\ln a)^2$$
$$-\frac{1}{4}(-1+\gamma-\ln 2)(\ln a)^3-\frac{(\ln a)^4}{16}\Big]a+O(a\ln a)+O\left(a^2(\ln a)^4\right),$$

$$I_3^{0,3}=\frac{3}{16}-\frac{45a}{32}+\Big[\frac{1}{64}\left(21-18\gamma+6\gamma^2+\pi^2+18\ln 2-12\gamma\ln 2+6\ln 2^2\right)(\ln a)^2$$
$$-\frac{1}{32}(3-2\gamma+2\ln 2)(\ln a)^3+\frac{(\ln a)^4}{64}\Big]a^2+O(a^2\ln a)+O\left(a^3(\ln a)^4\right),$$

$$I_4^{0,3}=\frac{1}{27}-\frac{65a}{864}+\frac{575a^2}{1728}$$
$$+\Big[\frac{\left(-85+66\gamma-18\gamma^2-3\pi^2-66\ln 2+36\gamma\ln 2-18\ln 2^2\right)(\ln a)^2}{1152}$$
$$-\frac{1}{576}(-11+6\gamma-6\ln 2)(\ln a)^3-\frac{(\ln a)^4}{384}\Big]a^3+O(a^3\ln a)+O\left(a^4(\ln a)^4\right),$$

$$I_5^{0,3}=\frac{3}{256}-\frac{175a}{13824}+\frac{865a^2}{55296}-\frac{5845a^3}{110592}$$
$$+\Big[\frac{\left(415-300\gamma+72\gamma^2+12\pi^2+300\ln 2-144\gamma\ln 2+72\ln 2^2\right)(\ln a)^2}{36864}$$
$$-\frac{(25-12\gamma+12\ln 2)(\ln a)^3}{9216}+\frac{(\ln a)^4}{3072}\Big]a^4+O(a^4\ln a)+O\left(a^5(\ln a)^4\right). \tag{B.9}$$

The case $n>0$ is obtained by the differentiation of these expressions according to (B.2).

Acknowledgments

The authors thank I M Sigal for many helpful discussions.

Work of PL, SD and NV was partially supported by NSF grants DMS 0719895 and DMS 0807131.

References

[1] Patlak C S 1953 Random walk with persistence and external bias *Bull. Math. Biophys.* **15** 311–38
[2] Keller E F and Segel L A 1970 Initiation of slime mold aggregation viewed as an instability *J. Theor. Biol* **26** 399–415
[3] Alt W 1980 Biased random walk models for chemotaxis and related diffusion approximations *J. Math. Biol.* **9** 147–77
[4] Herrero M A and Juan J L Velázquez 1996 Singularity patterns in a chemotaxis model *Math. Ann.* **306** 583–623
[5] Brenner M P, Levitov L S and Budrene E O 1998 Physical mechanisms for chemotactic pattern formation by bacteria *Biophys. J.* **74** 1677–93

[6] Brenner M P, Constantin P, Kadanoff L P, Schenkel A and Venkataramani S C 1999 Diffusion, attraction and collapse *Nonlinearity* **12** 1071–98

[7] Ben-Jacob E, Cohen I and Levine H 2000 Cooperative self-organization of microorganisms *Adv. Phys.* **49** 395–554

[8] Betterton M D and Brenner M P 2001 Collapsing bacterial cylinders *Phys. Rev.* E **64** 061904

[9] Velazquez J J L 2002 Stability of some mechanisms of chemotactic aggregation *SIAM J. Appl. Math.* **62** 1581–633

[10] Othmer H G and Hillen T 2002 The diffusion limit of transport equations II: chemotaxis equations *SIAM J Appl. Math.* **62** 1222–50

[11] Sire C and Chavanis P H 2002 Thermodynamics and collapse of self-gravitating Brownian particles in *d* dimensions *Phys. Rev.* E **66** 046133

[12] Erban R and Othmer H G 2005 From individual to collective behavior in bacterial chemotaxis *SIAM J Appl. Math.* **65** 361–91

[13] Newman T J and Grima R 2004 Many-body theory of chemotactic cell–cell interactions *Phys Rev.* E **70** 051916

[14] Lushnikov P M 2010 Critical chemotactic collapse *Phys. Lett.* A **374** 1678–85

[15] Dejak S I, Lushnikov P M, Ovchinnikov Yu N and Sigal I M 2012 On spectra of linearized operators for Keller–Segel models of chemotaxis *Physica* D **241** 1245–1254

[16] Dejak S I, Egli D, Lushnikov P M and Sigal I M 2013 On blowup dynamics in the Keller–Segel model of chemotaxis *St. Petersburg Math. J.* at press (arXiv:1304.1583)

[17] Raphael P and Schweyer R 2012 On the stability of critical chemotactic aggregation arXiv:1209.2517

[18] Herrero M A, Medina E and Velázquez J J L 1997 Finite-time aggregation into a single point in a reaction-diffusion system *Nonlinearity* **10** 1739–54

[19] Wolansky G 1992 On steady distributions of self-attracting clusters under friction and fluctuations *Arch. Ration. Mech. Anal.* **119** 355–91

[20] Chavanis P H and Sire C 2011 Exact analytical solution of the collapse of self-gravitating Brownian particles and bacterial populations at zero temperature *Phys. Rev.* E **93** 031131

[21] Biler P and Woyczynski W A 1998 Global and exploding solutions for nonlocal quadratic evolution problems *SIAM J. Appl. Math.* **59** 845–69

[22] Kuznetsov E A and Zakharov V E 2007 *Wave Collapse* (New York: World Scientific)

[23] Sulem C and Sulem P L 1999 *Nonlinear Schrödinger Equations: Self-Focusing and Wave Collapse* (New York: World Scientific)

[24] Alber M, Chen N, Glimm T and Lushnikov P M 2006 Multiscale dynamics of biological cells with chemotactic interactions: from a discrete stochastic model to a continuous description *Phys. Rev.* E **73** 051901

[25] Alber M, Chen N, Lushnikov P M and Newman S A 2007 Continuous macroscopic limit of a discrete stochastic model for interaction of living cells *Phys. Rev. Lett.* **99** 168102

[26] Lushnikov P M, Chen N and Alber M 2008 Macroscopic dynamics of biological cells interacting via chemotaxis and direct contact *Phys. Rev.* E **78** 061904

[27] Chiao R Y, Garmire I and Townes C H 1964 Self-trapping of optical beams *Phys. Rev. Lett.* **13** 479

[28] Vlasov S N, Petrishchev V A and Talanov V I 1971 Averaged description of wave beams in linear and nonlinear media *Izv. Vys. Uchebn. Zaved. Radiofizika* **14** 1353

[29] Zakharov V E 1972 Collapse of Langmuir waves *Sov. Phys.—JETP* **35** 908

[30] Zakharov V E and Kuznetsov E A 1986 Quasiclassical theory of three-dimensional wave collapse *Sov. Phys.—JETP* **64** 773–9

[31] Lushnikov P M 1995 Dynamic criterion for collapse *JETP Lett.* **62** 461–7

[32] Sulem C and Sulem P L 1999 *Nonlinear Schrödinger Equations: Self-Focusing and Wave Collapse* (New York: World Scientific)

[33] Sire C and Chavanis P H 2008 Critical dynamics of self-gravitating Langevin particles and bacterial populations *Phys. Rev.* E **78** 061111

[34] Fraiman G M 1985 Asymptotic stability of manifold of self-similar solutions on self-focusing *Sov. Phys.—JETP* **61** 228

[35] LeMesurier B J, Papanicolaou G, Sulem C and Sulem P L 1988 Focusing and multi-focusing solutions of the nonlinear Schrödinger equation *Physica* D **31** 78

[36] Landman M J, Papanicolaou G C, Sulem C and Sulem P L 1988 Rate of blowup for solutions of the nonlinear Schrödinger equation at critical dimension *Phys. Rev.* A **38** 3837–43

[37] Dyachenko S, Newell A C, Pushkarev A and Zakharov V E 1992 Optical turbulence: weak turbulence, condensates and collapsing fragments in the nonlinear Schrödinger equation *Physica* D **57** 96

[38] Fibich G and Papanicolaou G 1999 Self-focusing in the perturbed and unperturbed nonlinear Schrödinger equation in critical dimension *SIAM J. Appl. Math.* **60** 183

[39] Merle F and Raphael P 2006 On a sharp lower bound on the blow-up rate for the l^2 critical nonlinear Schrödinger equation *J. Am. Math Soc.* **19** 37
[40] Lushnikov P M, Dyachenko S A and Vladimirova N 2013 Beyond leading-order logarithmic scaling in the catastrophic self-focusing collapse of a laser beam in Kerr media *Phys. Rev.* A **88** 013845
[41] Talanov V I 1970 Focusing of light in cubic media *JETP Lett.* **11** 199–201
[42] Kuznetsov E A and Turitsyn S K 1985 Talanov transformations in self-focusing problems and instability of stationary waveguides *Phys. Lett.* A **112** 273–5
[43] Dyachenko S A, Lushnikov P M and Vladimirova N 2011 Logarithmic-type scaling of the collapse of Keller–Segel equation *AIP Conf. Proc.* **1389** 709–12
[44] Chavanis P H and Sire C 2006 Virial theorem and dynamical evolution of self-gravitating Brownian particles in an unbounded domain: I. Overdamped models *Phys. Rev.* E **73** 066103
[45] Lushnikov P M 2002 Collapse of Bose–Einstein condensate with dipole–dipole interactions *Phys. Rev.* A **66** 051601(R)
[46] Lushnikov P M 2010 Collapse and stable self-trapping for Bose–Einstein condensates with $1/r^b$ type attractive interatomic interaction potential *Phys. Rev.* A **82** 023615
[47] Lahaye T, Metz J, Fröhlich B, Koch T, Meister M, Griesmaier A, Pfau T, Saito H, Kawaguchi Y and Ueda M 2008 D-wave collapse and explosion of a dipolar Bose–Einstein condensate *Phys. Rev. Lett.* **101** 080401
[48] Sidorov Yu V, Fedoryuk M V and Shabunin M I 1985 *Lectures on the Theory of Functions of a Complex Variable* (Moscow: Mir)
[49] Olver F W J 1974 *Asymptotics and Special Functions* (New York: Academic)
[50] Berger M J and Colella P 1989 Local adaptive mesh refinement for shock hydrodynamics *J. Comput. Phys.* **82** 64–84
[51] http://fftw.org
[52] Hofer T, Sherratt J A and Maini P K 1995 Virial theorem and dynamical evolution of self-gravitating Brownian particles in an unbounded domain: I. Overdamped models *Physica* D **85** 425
[53] Luca M, Chavez-Ross A, Edelstein-Keshet L and Mogilner A 2003 Chemotactic signaling, microglia, and Alzheimer's disease senile plaques: is there a connection? *Bull. Math. Biol.* **65** 693
[54] Grima R 2005 Strong-coupling dynamics of a multicellular chemotactic system *Phys. Rev. Lett.* **95** 128103
[55] Gradshteyn I S and Ryzhik I M 2007 *Table of Integrals, Series, and Products* 7th edn (New York: Academic)
[56] Prudnikov A P, Marichev O I and Brychkov Yu A 1990 *Integrals and Series, Vol. 3: More Special Functions* (Newark, NJ: Gordon and Breach)